

Convex Active Contours with Locally Bias Field Estimator

Muhammad Salim Khan¹, Haider Ali², Noor Badshah³, Gohar Ayub Khan⁴

^{1,3}Department of Basic Sciences,

University of Engineering and Technology, Peshawar, Pakistan.

²Department of Mathematics,

University of Peshawar, Pakistan.

⁴Department of Physics,

University of Science and Technology Bannu, Pakistan.

Email: ^{1,2,3,4} salimgul.433@gmail.com, dr.haider@uop.edu.pk, noor2knoor@gmail.com, ghrayub@gmail.com

Received: 27 January, 2020 / Accepted: 11 September, 2020 / Published online: 10 October, 2020

Abstract. Intensity inhomogeneity or bias field in natural and medical images make image processing challenging. In this paper we have introduced a novel technique in which we first estimate the bias field using multi-scale filtering. Based on the bias field, the bias field corrected image is obtained which is used for accurate segmentation. For segmentation, a convex functional is proposed which is also suitable for multi-region segmentation. The proposed formulation is extended to vector-valued images and texture images. For comparison, the results are compared with state of the art models both qualitatively and quantitatively which validate strong enactment of the proposed formulation.

AMS (MOS) Subject Classification Codes: 35S29; 40S70; 25U09

Key Words: Calculus of Variation, Image segmentation, Euler's Lagrange equation, Texture Segmentation, Numerical methods.

1. INTRODUCTION

Segmentation aims to automatically divide an observed image into useful segments of features with sharp boundaries such as buildings, desks, people, trees, organs, cars or whatever are within a picture [22, 7, 8, 11, 15, 3, 17, 18, 5, 16, 6, 19]. In this paper, our main concern is multi-region image segmentation in presence of intensity inhomogeneity. The presence of intensity inhomogeneity in a given image greatly effects the performance of image segmentation models [9]. For piecewise smooth ideal image one can use Chan-Vese (CV) model [8] which is special case of Mumford Shah model [15]. The CV minimization

model is as follow:

$$F^{CV}(c_1, c_2, C) = \lambda_1 \int_{inside(C)} |u_0(\mathbf{x}) - c_1|^2 \mathbf{d}\mathbf{x} + \lambda_2 \int_{outside(C)} |u_0(\mathbf{x}) - c_2|^2 \mathbf{d}\mathbf{x},$$

$$+ \mu \text{length}(C) \quad (1. 1)$$

On the other hand, several recent works can be seen in the literature which extend the CV model for segmenting images with intensity inhomogeneity [1, 20, 21, 2, 14, 12, 9]. A well known example is the local binary fitting model (LBF) model [12] which proposes the following functional of minimization:

$$F_\epsilon^{LBF}(\phi, f_1, f_2) = \mu \int_{\Omega} \delta(\phi) |\nabla H| \mathbf{d}\mathbf{x} + \nu \int_{\Omega} (|\nabla \phi| - 1)^2 \mathbf{d}\mathbf{x} \quad (1. 2)$$

$$+ \lambda_1 \int \left[\int K_\sigma(\mathbf{x} - \mathbf{y}) |u_0(\mathbf{y}) - f_1(\mathbf{x})|^2 H(\phi(\mathbf{y})) \mathbf{d}\mathbf{y} \right] \mathbf{d}\mathbf{x}$$

$$+ \lambda_2 \int \left[\int K_\sigma(\mathbf{x} - \mathbf{y}) |u_0(\mathbf{y}) - f_2(\mathbf{x})|^2 (1 - H(\phi(\mathbf{y}))) \mathbf{d}\mathbf{y} \right] \mathbf{d}\mathbf{x}$$

where K_σ is the gaussian kernel having standard deviation σ , u_0 is given image, f_1 and f_2 , are the smooth functions which fits the given image locally inside and outside of the contour C respectively, are given by:

$$f_1(x) = \frac{K_\sigma(x) * I(x) H_\epsilon(\phi(x))}{K_\sigma(x) * H_\epsilon(\phi(x))}, \quad f_2(x) = \frac{K_\sigma(x) * I(x) (1 - H_\epsilon(\phi(x)))}{K_\sigma(x) * (1 - H_\epsilon(\phi(x)))}. \quad (1. 3)$$

In practical applications, the standard deviation of the Gaussian kernel plays an important role. It functions as a scale parameter that regulates the scalability of the area from the small neighborhood to the whole image domain[12]. It must be chosen according to the images. Too small a standard deviation will lead to an undesirable outcome, while too large a standard deviation can result in high computational costs. On the other hand the well-known Li-Kim model [13] for multi-region segmentation proposes the following functional of minimization

$$F^{LK}(c_1, c_2, \phi) = \lambda_1 \int_{\Omega} (u_0 - c_1)^2 \phi H_c(1 + \phi) \mathbf{d}\mathbf{x}$$

$$+ \lambda_2 \int_{\Omega} (u_0 - c_2)^2 \phi H_c(1 - \phi) \mathbf{d}\mathbf{x} \quad (1. 4)$$

where

$$H_c(z) = \frac{1 + z}{2}, \quad (1. 5)$$

is not designed for images with intensity variation in the objects and background. Similar is the behavior of the latest Wu-He model [22] which minimize as follows:

$$F^{WH}(\phi, c_1, c_2) = \lambda \int_{\Omega} \frac{(u_0 - c_1)^2}{c_1^2} (\phi + 1)^2 \mathbf{d}\mathbf{x},$$

$$+ \int_{\Omega} \frac{(u_0 - c_2)^2}{c_2^2} (\phi - 1)^2 \mathbf{d}\mathbf{x}, \quad (1. 6)$$

where $\lambda > 0$.

For bias field correction and joint segmentation Li et al proposed model [10] which minimize as follows:

$$F^{BF}(\phi, b, c) = \int \int K_\sigma(\mathbf{x} - \mathbf{y}) |u_0(\mathbf{y}) - b(\mathbf{x})c_1|^2 M_1(\phi(\mathbf{y})) d\mathbf{y} d\mathbf{x} + \int \int K_\sigma(\mathbf{x} - \mathbf{y}) |u_0(\mathbf{y}) - b(\mathbf{x})c_2|^2 M_2(\phi(\mathbf{y})) d\mathbf{y} d\mathbf{x} \quad (1.7)$$

where $M_1(\phi(\mathbf{x})) = H(\phi(\mathbf{x}))$, $M_2(\phi(\mathbf{x})) = 1 - H(\phi(\mathbf{x}))$ and b is the bias field.

By minimization the energy functional $F^{BF}(\phi, b, c)$ with respect to b we obtained:

$$\hat{b} = \frac{(u_0 J^1) * K_\sigma}{J^2 * K_\sigma}, \quad (1.8)$$

In the same way minimization of $\hat{c} = (\hat{c}_1, \hat{c}_2)$ is given by:

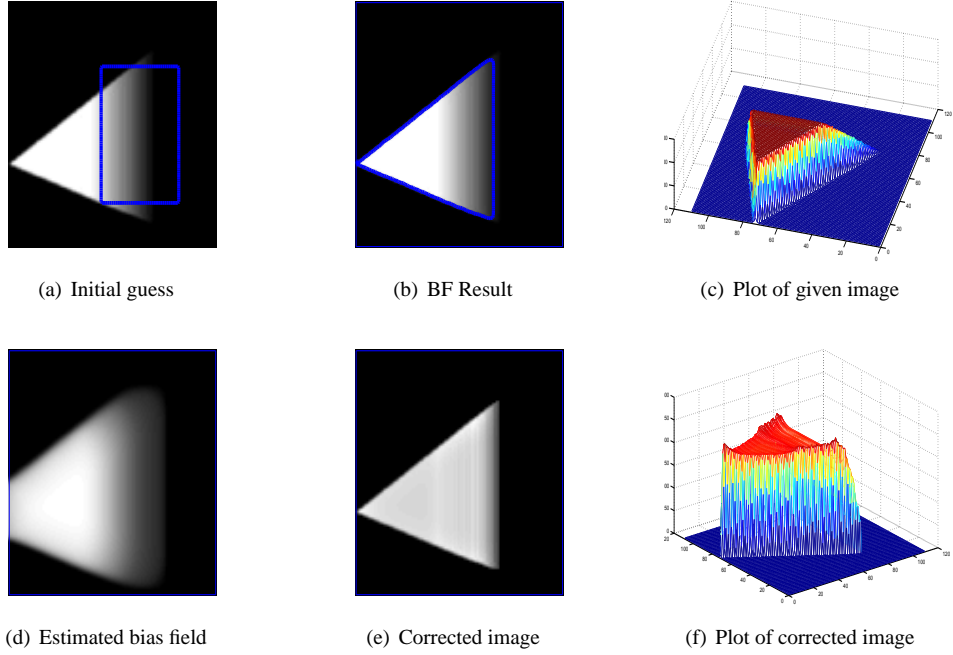


Figure 1: Satisfactory performance of the BF model in an ideal given image where bias field is slowly varying.

$$\hat{c}_i = \frac{\int_{\Omega} (b * K_\sigma) u_0(\mathbf{x}) M_i(\phi) d\mathbf{x}}{\int_{\Omega} (b^2 * K_\sigma) M_i(\phi) d\mathbf{x}}, \quad i = 1, 2. \quad (1.9)$$

It is assumed that the bias field b is window-wise constant and smoothly varying function. The BF model works efficiently when given images are in complete concordance with its assumptions. This phenomenon can be witnessed in Fig. 1. That is, when bias field b is smoothly varying function over image domain and the bias field free version of given image is piece-wise constant. However, the BF model may not work well when neither bias field b is smoothly varying function (i.e when it is not neighborhood wise constant) or the ideal bias field free image is not piece-wise constant. This phenomenon can be witnessed in Fig. 17. In other words, the segmentation process in the BF model is dependent on bias field estimation and vice versa. Thus if segmentation is not accurate then the bias field is also not accurate and converse is also true. Thus in this paper we have introduced a novel technique in which we first estimate the bias field using multi-scale filtering. Based on the bias field, the bias field corrected image is obtained which is used for accurate segmentation. For segmentation, a convex functional is proposed which is also suitable for multi-region segmentation. The proposed formulation is extended to vector-valued images and texture images. For comparison, the results are compared with state of the art models both quantitatively and qualitatively which validate robust enactment of the proposed formulation.

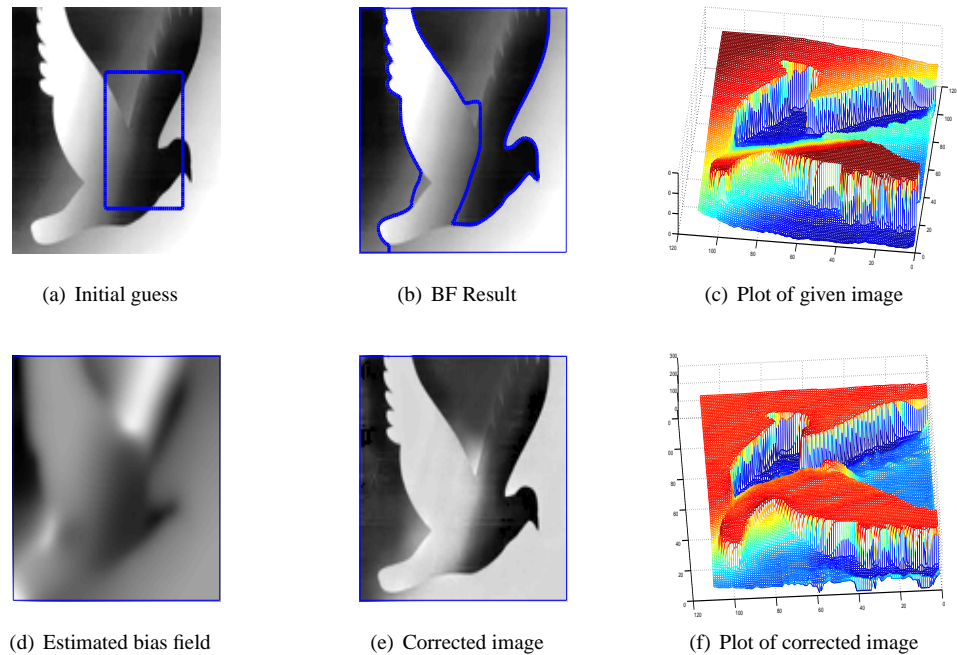


Figure 2: Unsatisfactory performance of the BF model in a given image where bias field is not slowly varying.

The organization of the remainder of this paper is as follows. In section 2 we discuss our proposed model. In 3 we extend our model for segmenting textural images. In section 4 we give experimental evidence of the proposed model. Finally, conclusion is made in section 5.

2. THE PROPOSED METHOD

In this section we give step by step basic idea behind our technique for estimation of bias field and segmentation of images with intensity inhomogeneity.

2.1. Bias Field Estimator. In order to tackle intensity inhomogeneities or bias field in image segmentation, our technique is based on a well-known multiplicative image model

$$u_0 = bJ + N,$$

where the desired clean image J is corrupted by N additive noise and b intensity inhomogeneity, the obtained image is u_0 . When the factor of noise is ignored, the obtained image u_0 is representation in the form

$$u_0 = bJ. \quad (2.10)$$

In order to get the ideal image J from Eq. 2.10, the bias field b or at least its ap-

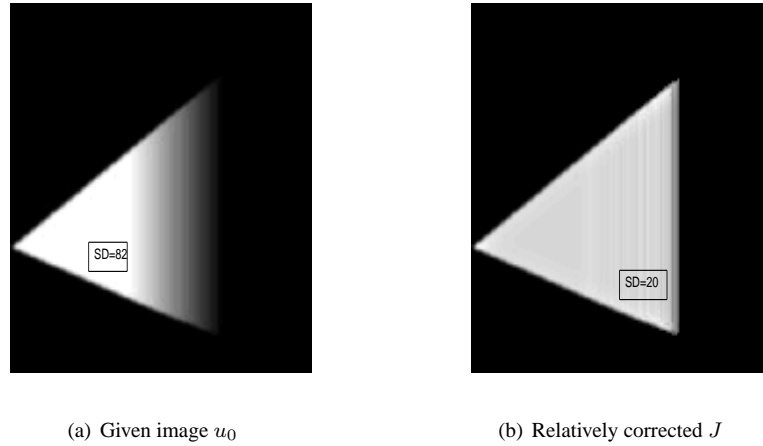


Figure 3: Given figure demonstrates the given image and relatively corrected image.

proximation must be known and vice versa. The main difference between a given image u_0 and bias corrected image J is that the intensities within each tissue/object become quite homogeneous in J . To measure homogeneity in intensities of objects/tissues, variance (Var) or standard deviation (SD) can be employed. The lesser Var and SD indicate the consistency/homogeneity in intensities in regions of a given image. This phenomena can be witnessed in Fig. 3, where the object/region (a triangle) in given image u_0 (Fig.

3(a) has higher intensity inhomogeneity or bias field as compared to triangular region in J (Fig. 3(b)). Consequently the region in u_0 has large SD which is 82 than the SD in J which is 20. Thus one key to bias field correction or intensity inhomogeneity reduction is local Var or local SD minimization. For local region or patch in a given image we consider a circular neighborhood with radius (say) \mathbf{r} centered at each point $\mathbf{x} \in \Omega$ defined by $N(\mathbf{x}) = \{\mathbf{y} \in \Omega : |\mathbf{x} - \mathbf{y}| \leq \mathbf{r}\}$. We denote the local variance and local mean in neighborhood $N(\mathbf{x})$ by $Var_{N(\mathbf{x})}$ and $\mu_{N(\mathbf{x})}$. Now by scaling property of variance and considering given image u_0 as random variable, we can write

$$Var_{N(\mathbf{x})}\left(\frac{u_0}{\mathbf{a}}\right) = \frac{Var_{N(\mathbf{x})}(u_0)}{\mathbf{a}^2} \quad (2. 11)$$

where \mathbf{a} is any real number. Left hand side of Eq. (2. 16) is variance of the scaled image $\frac{u_0}{\mathbf{a}}$, scaled with some constant \mathbf{a} in an arbitrary patch/neighbourhood $N(\mathbf{x})$, whereas the right hand side is the variance of the original image u_0 divided by \mathbf{a}^2 . It clearly illustrates that the variance of the scaled image $\frac{u_0}{\mathbf{a}}$ is less than the variance of u_0 . That is,

$$Var_{N(\mathbf{x})}\left(\frac{u_0}{\mathbf{a}}\right) < Var_{N(\mathbf{x})}(u_0) \quad (2. 12)$$

In other words, if a given bias field effected image u_0 is properly scaled then its intensity variation in objects/regions will be minimum and in this way the resultant image $\left(\frac{u_0}{\mathbf{a}}\right)$ will be having relatively less intensity inhomogeneity. It is important to point out that the scaling constant \mathbf{a} is not fixed over all image domain, in fact it is varying over image domain but constant in every neighborhood $N(\mathbf{x})$. To find a suitable value for the scaling constant \mathbf{a} , we define squared coefficient of variation of u_0 in $N(\mathbf{x})$ [3]:

$$CoV_{N(\mathbf{x})}^2(u_0) = \frac{Var_{N(\mathbf{x})}(u_0)}{\left(\mu_{N(\mathbf{x})}(u_0)\right)^2}. \quad (2. 13)$$

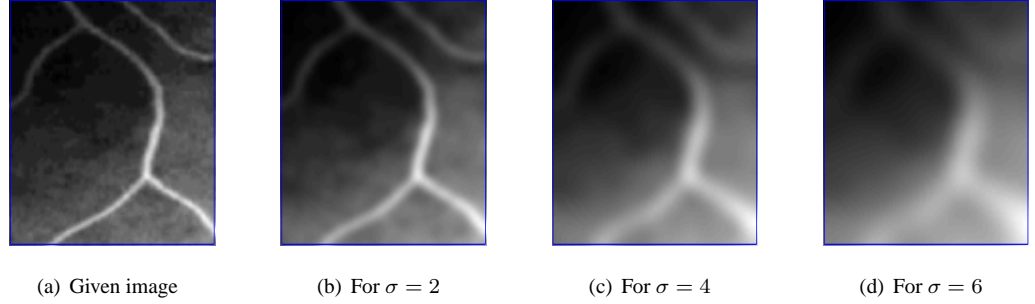
Similar to the inequality (2. 12), we have the following inequality

$$CoV_{N(\mathbf{x})}^2\left(\frac{u_0}{\mathbf{a}}\right) < CoV_{N(\mathbf{x})}^2(u_0) \quad (2. 14)$$

which also validates that the intensities of scaled image $\left(\frac{u_0}{\mathbf{a}}\right)$ are more consistent than the intensities of a given image u_0 in arbitrary neighborhood $N(\mathbf{x})$. Moreover, the last inequality (2. 14) also gives a suitable choice of the scaling constant which is $\mathbf{a} \cong \mu_{N(\mathbf{x})}(u_0)$. For numerical estimation of the quantity $\mathbf{a} \cong \mu_{N(\mathbf{x})}(u_0)$ in every neighborhood $N(\mathbf{x})$ of given image u_0 , we define the following mean filter type quantity:

$$u_S = \frac{u_0 * K_\sigma}{1 * K_\sigma}. \quad (2. 15)$$

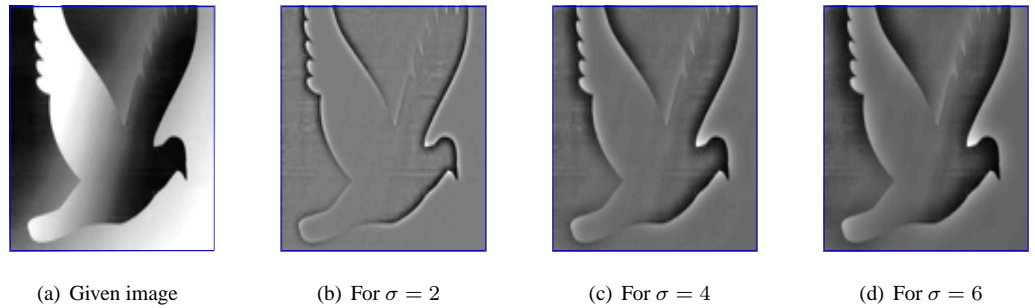
The idea behind u_S is similar to the neighborhood-wise constant (mean) quantities f_1 and f_2 defined in Eq. (1. 3). The f_1 and f_2 fits a given image in foreground and background respectively. On the other hand the term in Eq. (2. 15) fits given image u_0 over all domain Ω . For different values of σ , the mean fitting image u_S can be seen in Fig. 4. The Fig. 4(d) shows quit clear intensity distribution of given image u_0 . Now to get a scaled image

Figure 4: The effect of the values of σ in Eq. (2. 15)

$\mathbf{a} \cong \mu_{N(\mathbf{x})}(u_0)$ which is having less intensity variation in foreground and background, we at once can write:

$$\left(\frac{u_0}{a}\right)_{N(\mathbf{x})} = \left(\frac{u_0}{u_S}\right)_{N(\mathbf{x})}; \forall \mathbf{x} \in \Omega, \quad (2. 16)$$

where the size/radius of $N(\mathbf{x})$ is decided by tuning the parameter σ . The effect of σ on the scaled image $\frac{u_0}{u_S}$ in Eq. (2. 16) and in Fig. 5. It can be witnessed that if σ is too small such as 2, then variation in scaled image $\frac{u_0}{u_S}$ reduces but contrast in foreground and background also reduces.

Figure 5: The effect of the values of σ on scaled image $\frac{u_0}{u_S}$

2.2. Relation of Scaled Image $\frac{u_0}{u_S}$ and Bias Field Model. In contrast with the given image u_0 with intensity inhomogeneity, scaled image $\frac{u_0}{u_S}$ is a better approximation of ideal

image J in Eq. (2. 10). That is

$$C_k \frac{u_0}{u_S} \cong J, \quad (2. 17)$$

where C_k is a positive constant for adjusting/rescaling intensities (255 or $mean(u_0)$ for instance). Similarly, the mean filter type approximation u_S of u_0 can also be related with the bias field b in Eq. (2. 10). That is $u_S \cong b$, [9]. Thus we can write at once

$$u_0 = bJ \cong u_S \left(C_k \frac{u_0}{u_S} \right). \quad (2. 18)$$

2.3. Benefits of Scaled Image $\left(C_k \frac{u_0}{u_S} \right)$ Over J of BF Model. The classical BF model in Eq. (1. 7) may work well in ideal images and produce reasonable ideal image J and better segmentation result as shown in Fig. 1. However, when images are not ideal or according to the model assumption then both J and segmentation are not true as shown in Fig. 17. In contrast, in our method, bias field corrected image $J \cong \left(C_k \frac{u_0}{u_S} \right)$ is pre computed and is independent of segmentation process, whereas segmentation is dependent on it. Performance of the new enhanced image $J \cong \left(C_k \frac{u_0}{u_S} \right)$ can be seen for gray and color images in Figs. 6 and 7. It can be seen that the proposed formulation tackles the intensity inhomogeneity in images. Moreover, it can be seen in Figs. 6(i) and 7(a), that the proposed technique also tackles clutter backgrounds and light reflectance in images.

2.4. Convex Segmentation Formulation. In this section we present a convex and non convex variational models for efficiently segmenting images with intensity inhomogeneity, clutter backgrounds and multi-regions. We propose the following functional of minimization:

$$F^{KBA}(c_1, c_2, \phi) = \lambda_1 \int_{\Omega} \left(C_k \frac{u_0}{u_S} - c_1 \right)^2 \phi H_c(1 + \phi) \mathbf{d}\mathbf{x} + \lambda_2 \int_{\Omega} \left(C_k \frac{u_0}{u_S} - c_2 \right)^2 \phi H_c(1 - \phi) \mathbf{d}\mathbf{x}, \quad (2. 19)$$

where H_c is heaviside function defined in Eq. (1. 5). Our proposed model is designed to reduced the intensity inhomogeneity and capture boundaries of each and every object in a given image $u_0(\mathbf{x})$. The minimizers of our proposed model c_1, c_2 can be written as:

$$c_1(\phi) = \frac{\int_{\Omega} C_k \frac{u_0}{u_S} H_c(\phi) \mathbf{d}\mathbf{x}}{\int_{\Omega} H_c(\phi) \mathbf{d}\mathbf{x}} \quad c_2(\phi) = \frac{\int_{\Omega} C_k \frac{u_0}{u_S} (1 - H_c(\phi)) \mathbf{d}\mathbf{x}}{\int_{\Omega} (1 - H_c(\phi)) \mathbf{d}\mathbf{x}}. \quad (2. 20)$$

The gradient descent formulation of our proposed model is given by:

$$\begin{aligned} \frac{\partial \phi}{\partial t} = & \left[\lambda_1 \left(C_k \frac{u_0}{u_S} - c_1 \right)^2 + \lambda_2 \left(C_k \frac{u_0}{u_S} - c_2 \right)^2 \right. \\ & \left. + \left(\lambda_1 \left(C_k \frac{u_0}{u_S} - c_1 \right) - \lambda_2 \left(C_k \frac{u_0}{u_S} - c_2 \right) \right) \phi \right] \end{aligned} \quad (2. 21)$$

The proposed joint bias field correction and segmentation formulation can be implemented in the following segmentation frame work.

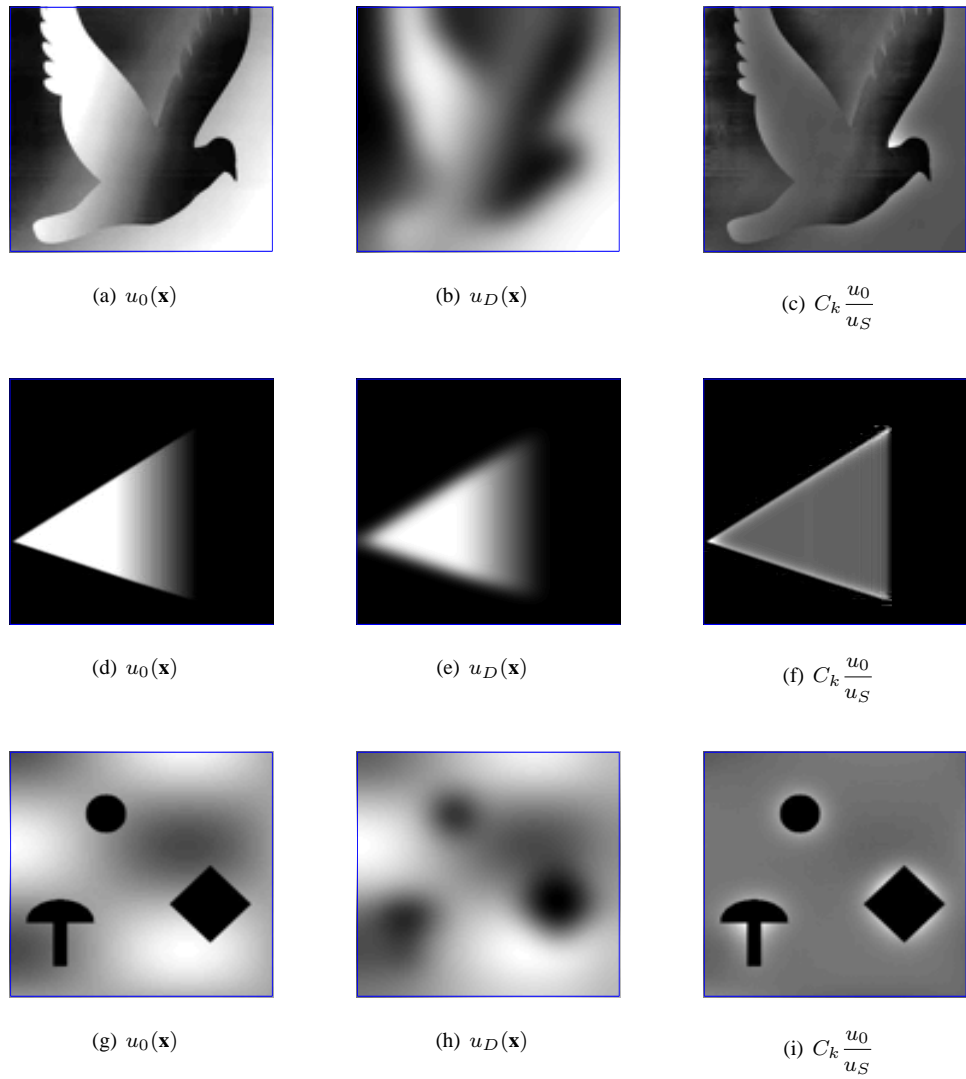


Figure 6: Given figure demonstrates the dual filter formulation in intensity inhomogeneity reduction. First column represent the given image, second column represent estimated intensity inhomogeneity and third column represent corrected image.

Below, the key steps of the proposed model for two phase gray images are presented as follows:

Algorithm to solve (2. 21) _____

Step 1. Insert the provided image $u_0(\mathbf{x})$ and customize the initial contour.

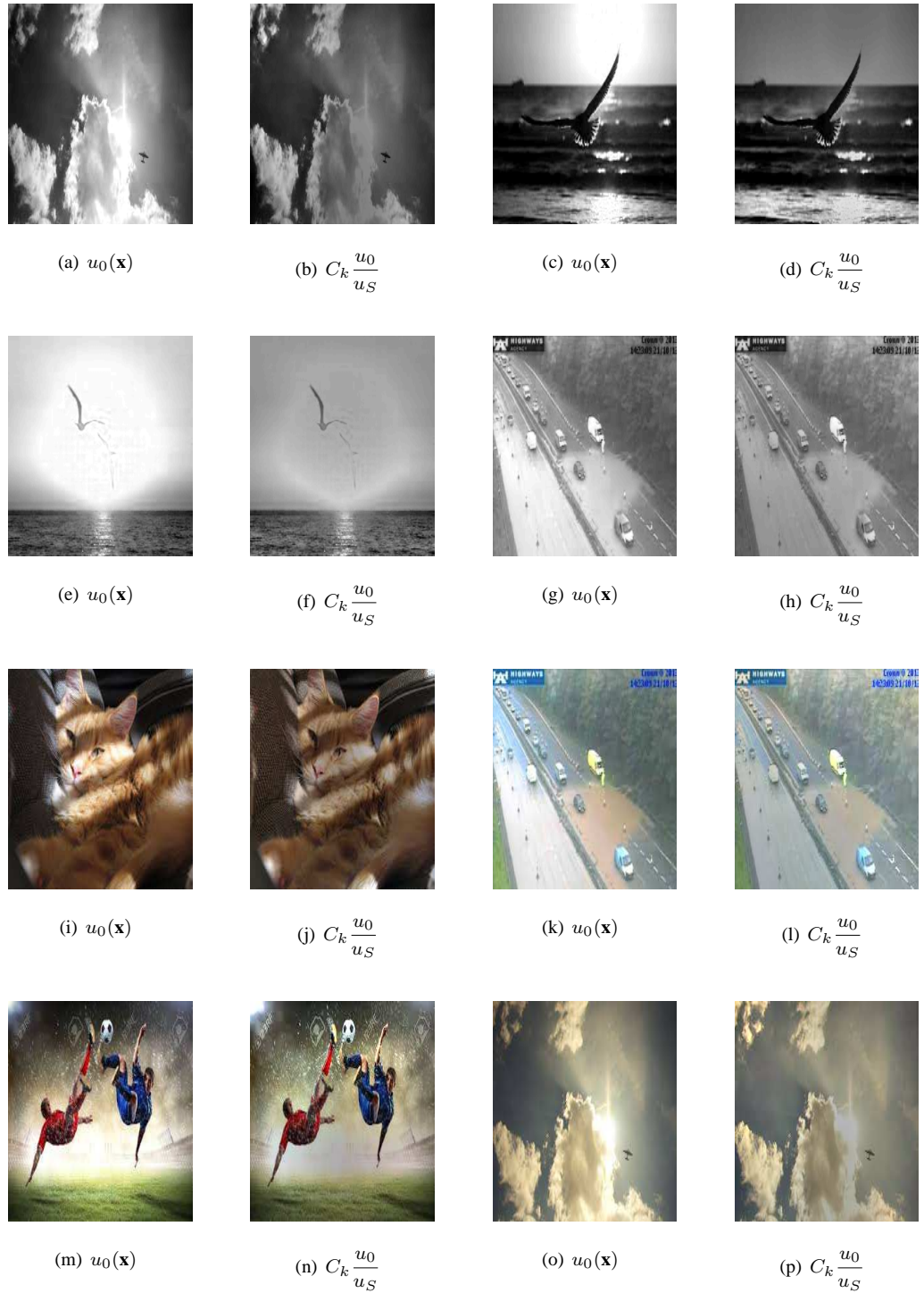


Figure 7: Results of dual filter formulation.

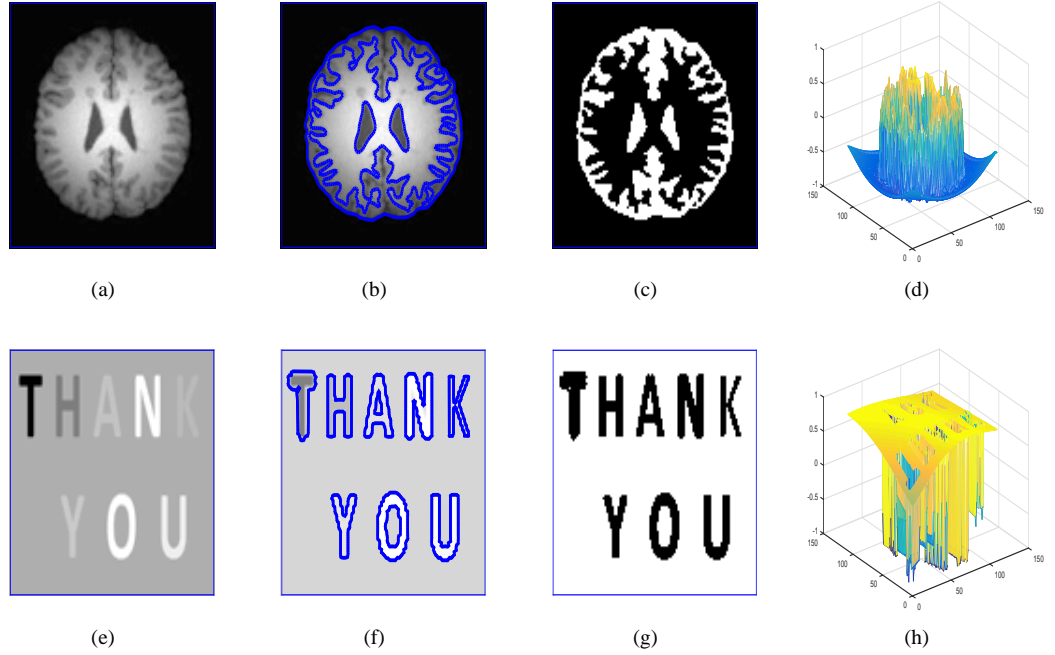


Figure 8: Segmentation result of the proposed KBA with intensity inhomogeneity.

Step 2. Obtain $C_k \frac{u_0}{u_S}$.

Step 3. c_1 and c_2 are computed using (2. 20).

Step 4. ϕ is evolved using (2. 21).

Step 5. If ϕ converges, stop; else return to Step 3.

Next we are expanding our proposed model for vector-based images

2.5. Vector-Valued KBA Model. In the case of vector-valued images, the energy functionality of our proposed model is as follows:

$$\begin{aligned}
 F^{VVKBA}(c_{1i}, c_{2i}, C) &= \frac{1}{N} \int_{inside(C)} \sum_{i=1}^N \lambda_i^+ |(C_k \frac{u_0}{u_S})_i - c_{1i}|^2 \phi H_c(1 + \phi) \mathbf{d}\mathbf{x} \\
 &+ \frac{1}{N} \int_{outside(C)} \sum_{i=1}^N \lambda_i^- |(C_k \frac{u_0}{u_S})_i - c_{2i}|^2 \phi H_c(1 - \phi) \mathbf{d}\mathbf{x}
 \end{aligned}
 \tag{2. 22}$$

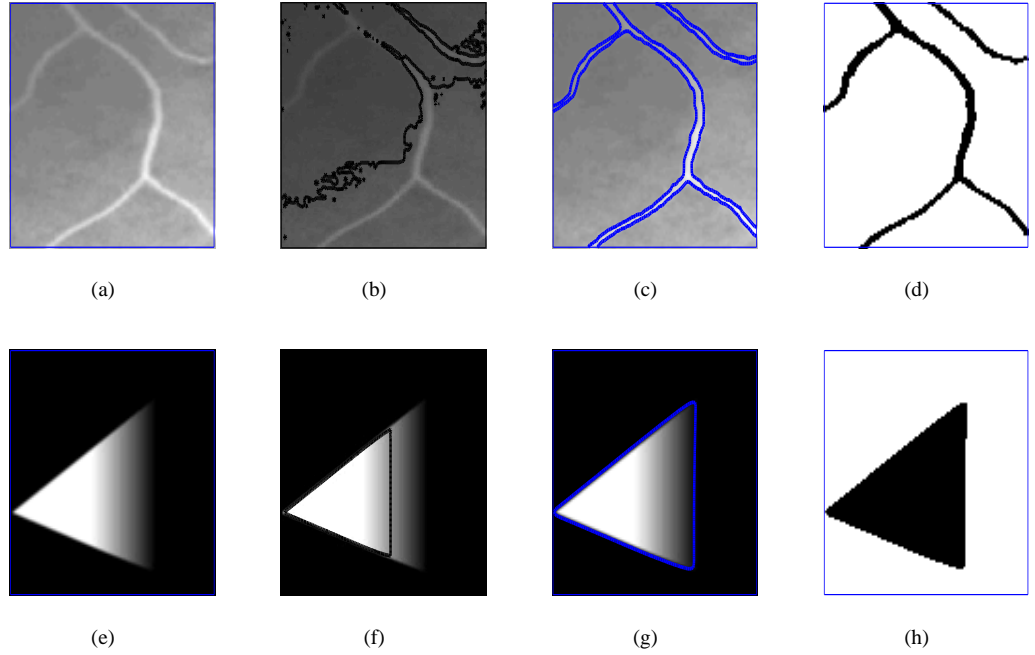


Figure 9: Given figure demonstrates the result of WH and proposed model on two different images suffered from intensity inhomogeneity. First, second and third columns represent the given image, result of WH model and KBA model, respectively. While the fourth column shows the segmented result of KBA model.

where i represents i th channel of a given vector valued image.

Minimizing the Eq. (2. 22) for c_{1i} we get.

$$c_{1i}(\phi) = \frac{\int_{\Omega} (C_k \frac{u_0}{u_S})_i(\mathbf{x}) \phi H_c(1 + \phi) \mathbf{d}\mathbf{x}}{\int_{\Omega} \phi H_c(1 + \phi) \mathbf{d}\mathbf{x}} \quad (2. 23)$$

Again by minimizing Eq. (2. 22) with respect to c_{2i} we get.

$$c_{2i}(\phi) = \frac{\int_{\Omega} (C_k \frac{u_0}{u_S})_i(\mathbf{x}) \phi H_c(1 - \phi) \mathbf{d}\mathbf{x}}{\int_{\Omega} \phi H_c(1 - \phi) \mathbf{d}\mathbf{x}} \quad (2. 24)$$

The following PDEs is obtained by minimizing with respect to ϕ

$$\begin{aligned} \frac{\partial \phi}{\partial t} = & \left[\frac{1}{N} \sum_{i=1}^N \lambda_i^+ \left((C_k \frac{\hat{u}_0}{u_S})_i(\mathbf{x}) - c_{1i} \right)^2 + \frac{1}{N} \sum_{i=1}^N \lambda_i^- \left((C_k \frac{\hat{u}_0}{u_S})_i(\mathbf{x}) - c_{2i} \right)^2 \right. \\ & \left. + \left(\frac{1}{N} \sum_{i=1}^N \lambda_i^+ \left((C_k \frac{\hat{u}_0}{u_S})_i(\mathbf{x}) - c_{1i} \right) - \frac{1}{N} \sum_{i=1}^N \lambda_i^- \left((C_k \frac{\hat{u}_0}{u_S})_i(\mathbf{x}) - c_{2i} \right) \right) \phi \right] \quad (2. 25) \end{aligned}$$

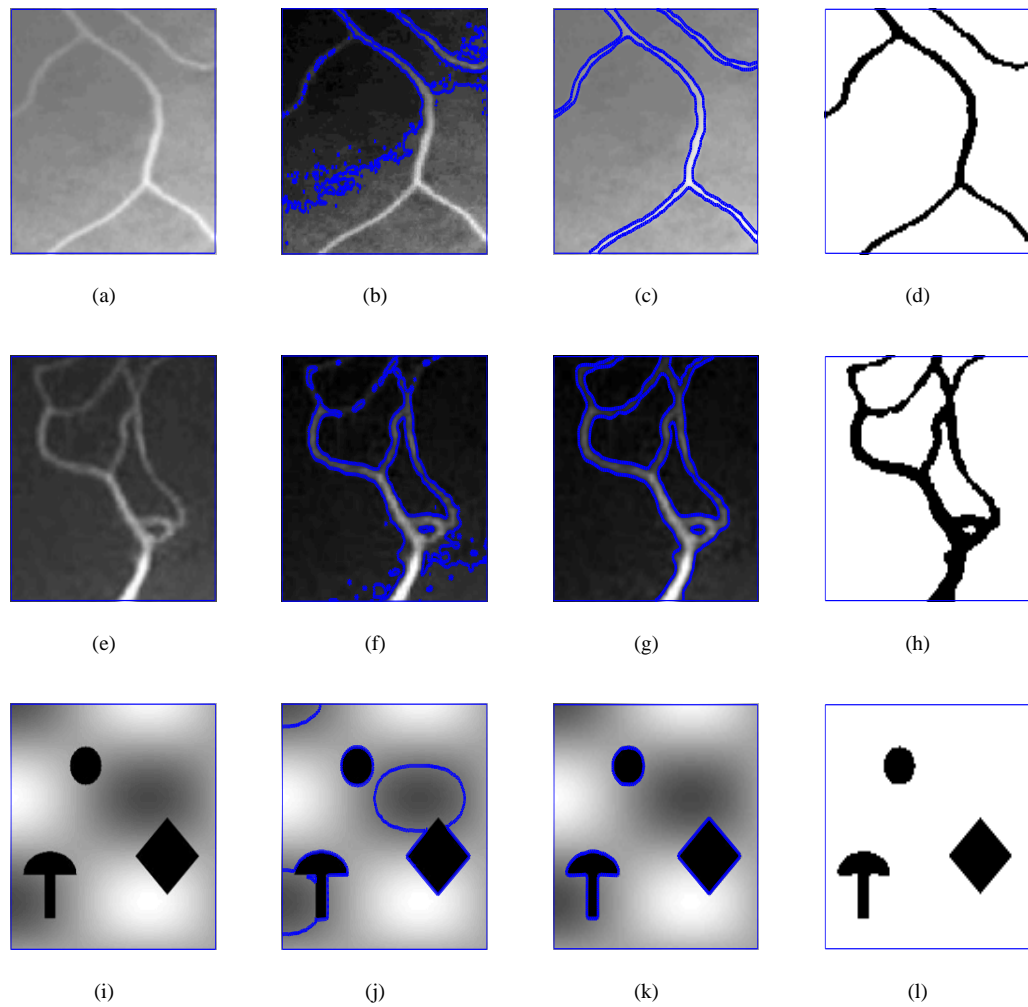


Figure 10: Given figure demonstrates the result of Li-Kim and proposed model on three different images suffered from intensity inhomogeneity. First, second and third columns represent the given image, result of Li-Kim model and KBA model, respectively. While the forth column shows the segmented result of KBA model.

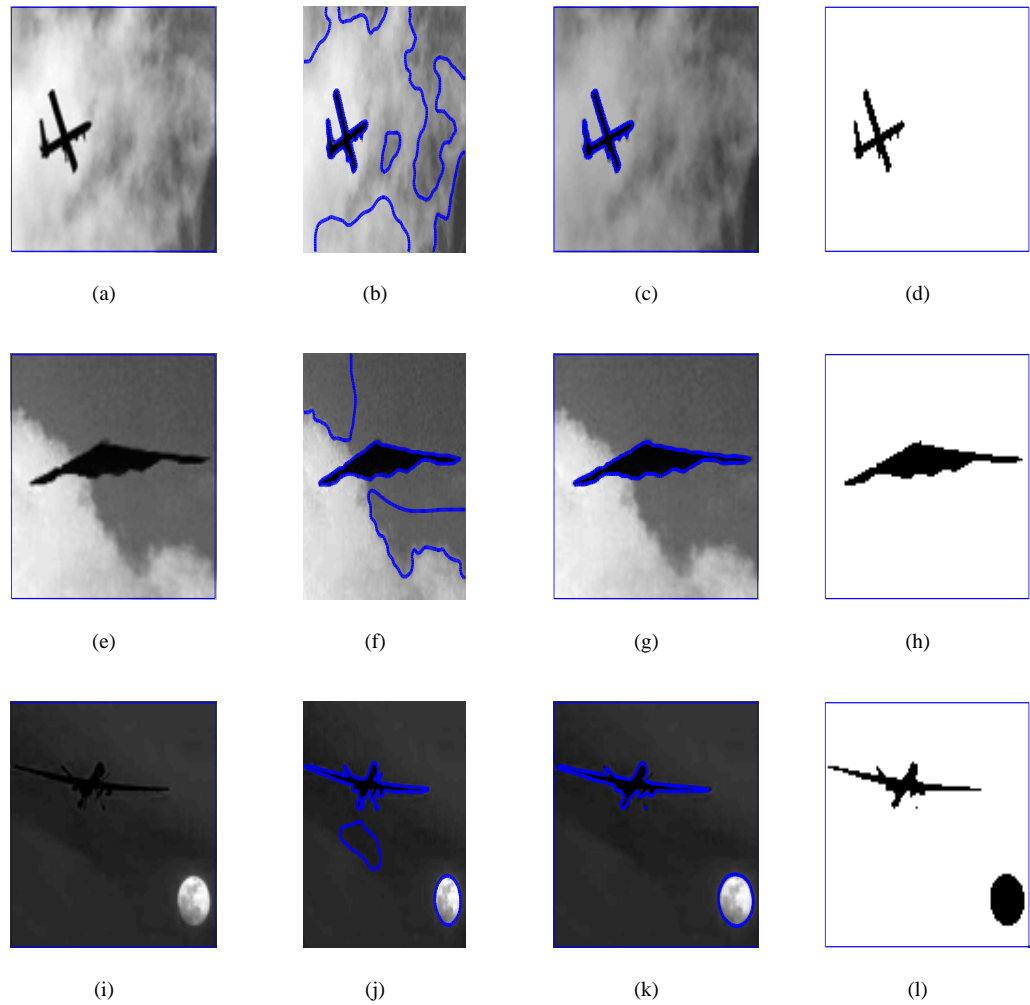


Figure 11: Given figure demonstrates the result of LBF and proposed model on three different images suffered from intensity inhomogeneity. First, second and third columns represent the given image, result of LBF model and KBA model, respectively. While the fourth column shows the segmented result of KBA model.

3. TEXTURE IMAGE SEGMENTATION

Here we extend our proposed model for texture image segmentation based on L_0 gradient norm and extended structure tensor (EST) [14]. The objective function of the L_0

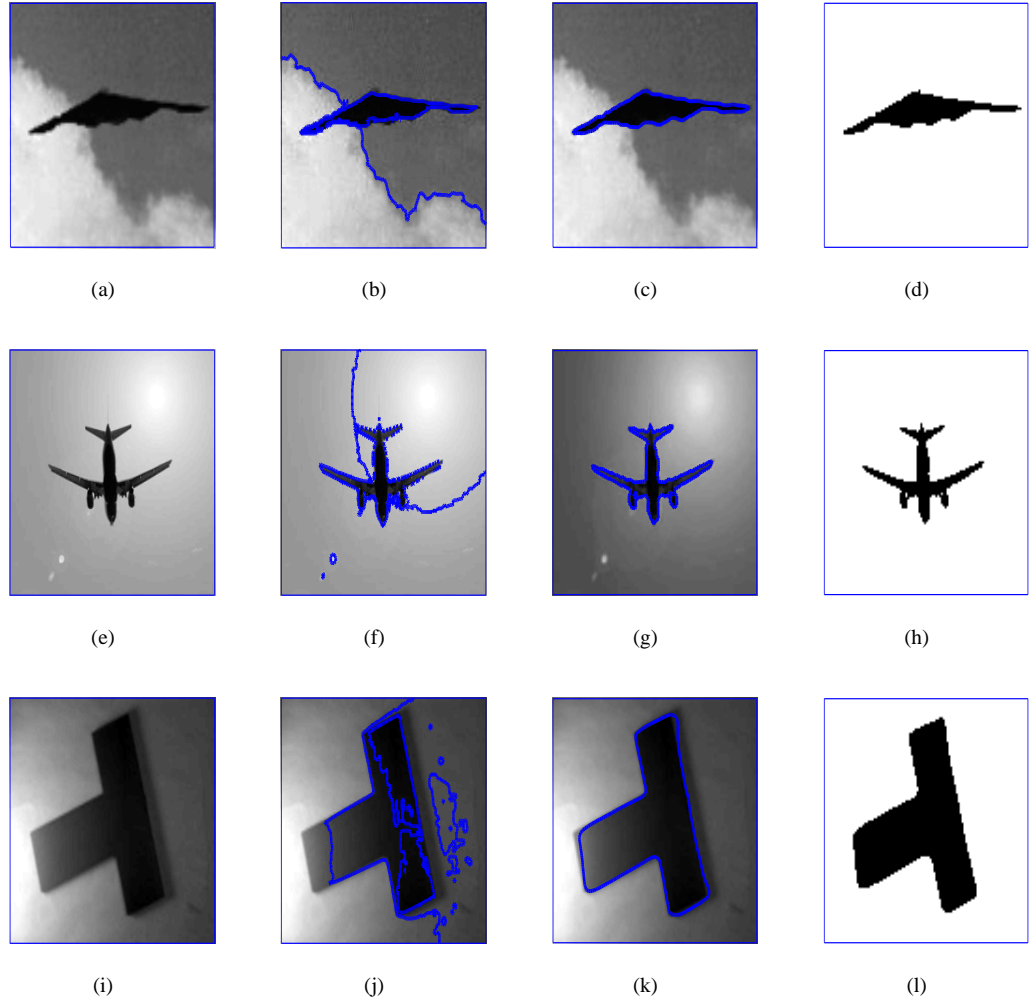


Figure 12: Given figure demonstrates the result of Li-Kim and proposed model on three different images suffered from intensity inhomogeneity. First, second and third columns represent the given image, result of Li-Kim model and KBA model, respectively. While the forth column shows the segmented result of KBA model.

gradient minimization is as:

$$\min_{S,h,v} \left\{ \sum_p (S_p - u_{0p})^2 + \lambda C(h,v) + \beta ((\partial_x S_p - h_p)^2 + (\partial_y S_p - \mu_p)^2) \right\}, \quad (3.26)$$

where $C(h,v) = \#\{p : |h_p| + |v_p| \neq 0\}$ and h_p, v_p are auxiliary variable corresponding to $\partial_x S_p$ and $\partial_y S_p$ respectively, β is an automatically adapting parameter to control

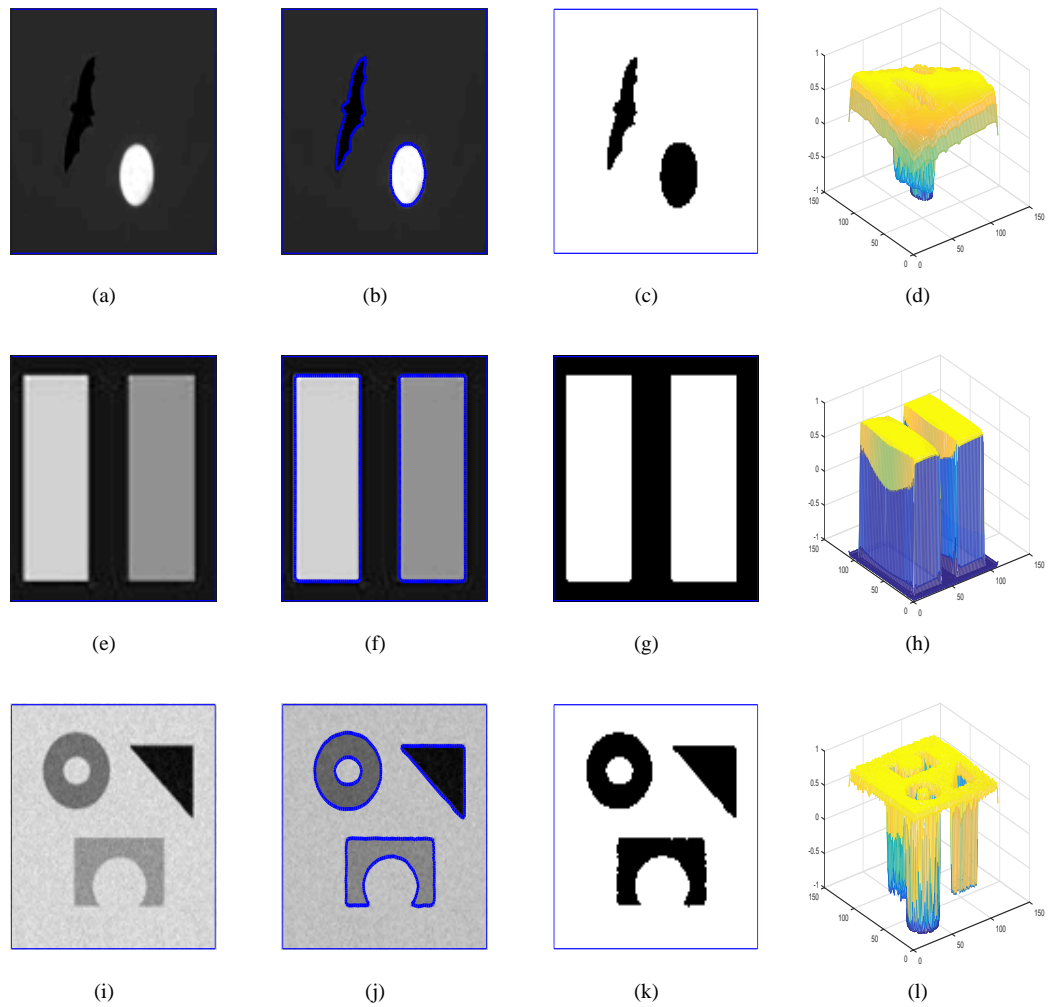


Figure 13: Segmentation result of proposed KBA model on multi-object images .

the similarity between (h, v) and their corresponding gradient. The functional in (3. 26) was proposed to preserve edges and to smooth a given image. This concept is helpful in segmentation to smooth the unnecessary noisy features and to make prominent the meaningful edges. On the other hand to smooth the textural features for efficient segmentation, extended structure tensor (EST) were introduced.

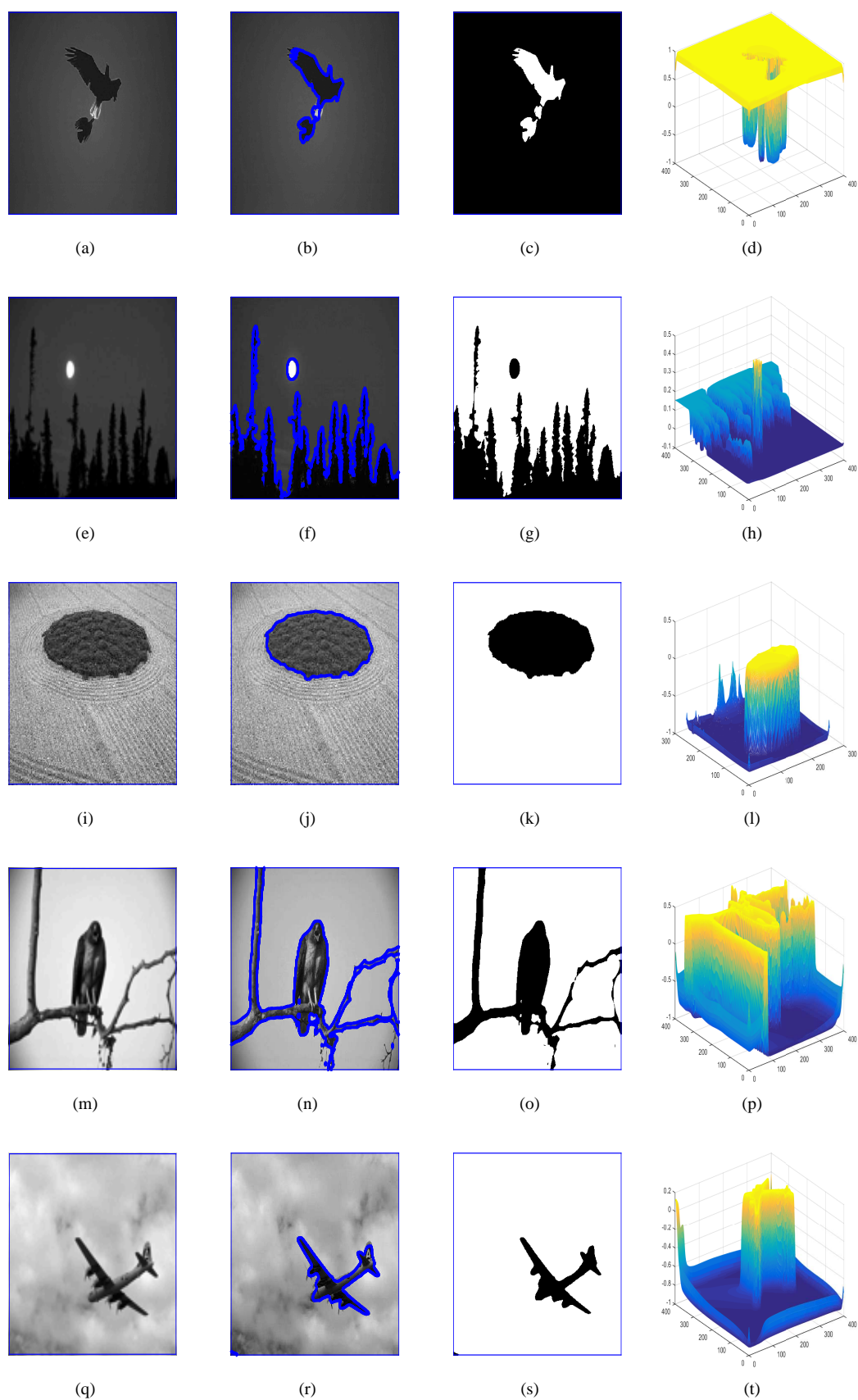


Figure 14: Segmentation result of the proposed KBA model on Berkeley Segmentation Dataset .

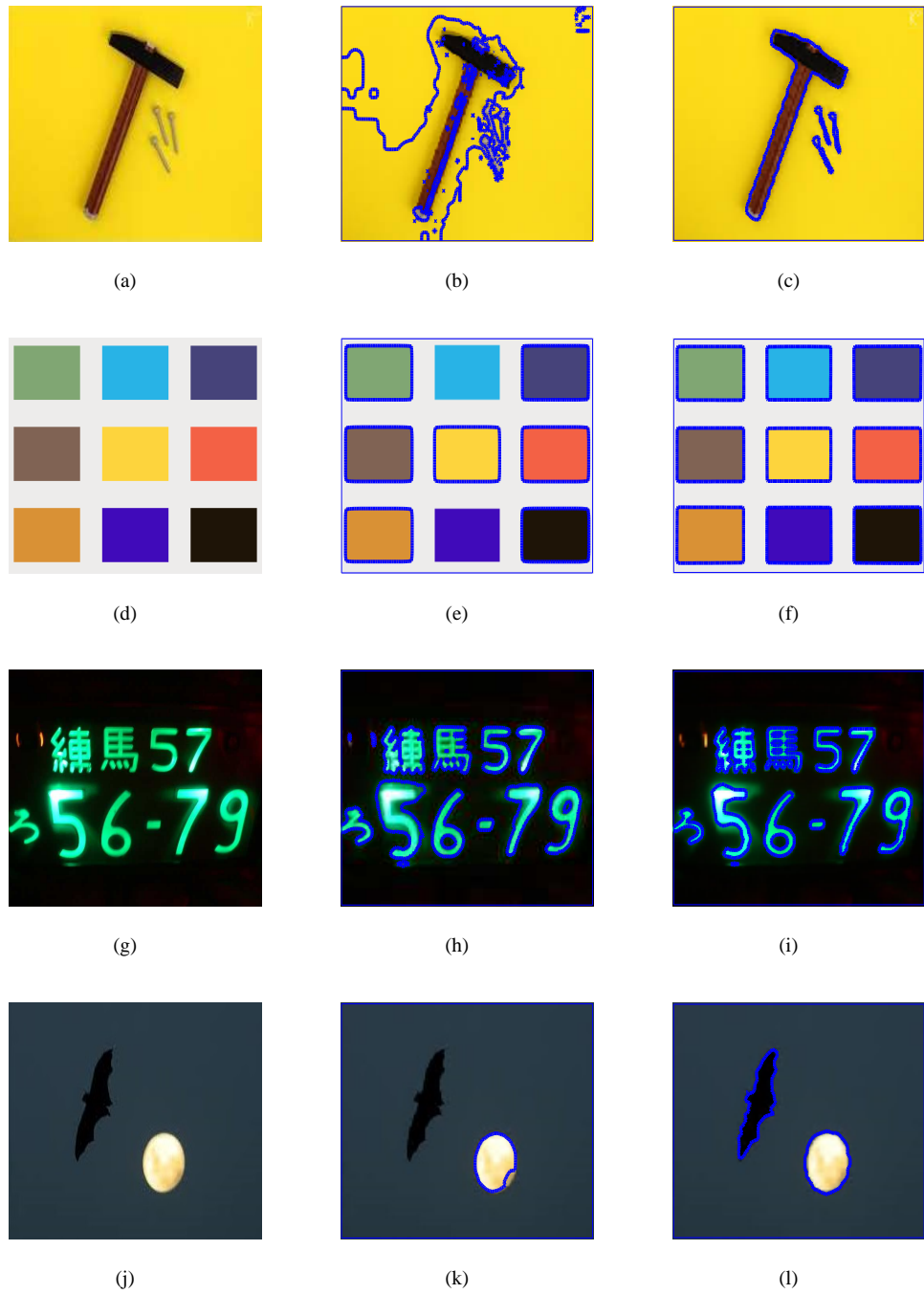


Figure 15: Given figure demonstrates the result of VVCV and proposed VVKBA model on four different images suffered from intensity inhomogeneity. First, second and third columns represent the given image, result of VVCV model and VVKBA model, respectively.

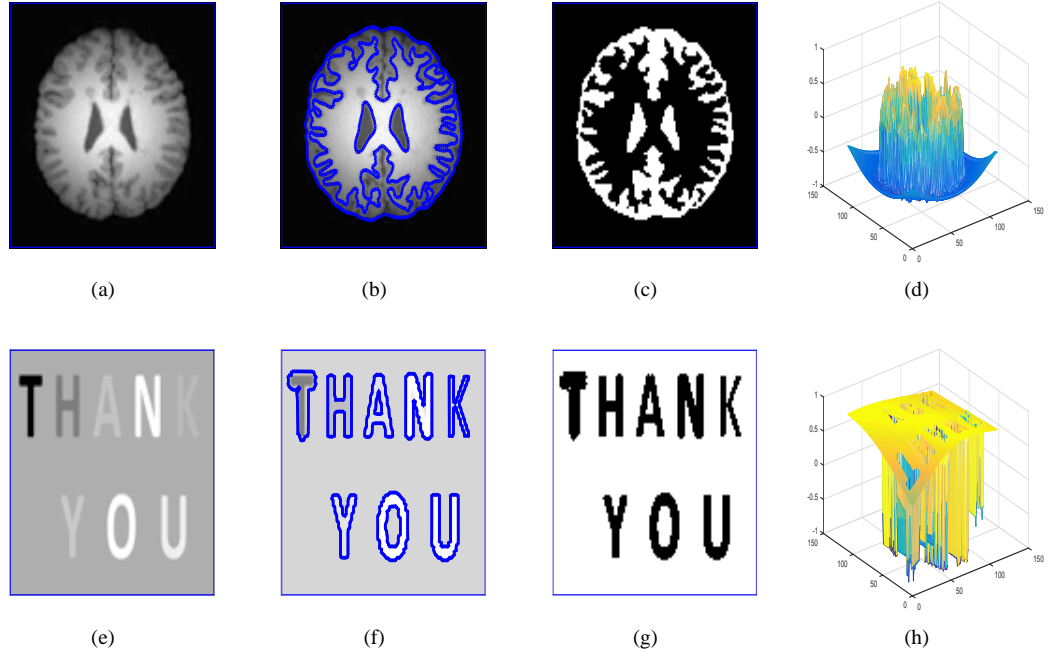


Figure 16: Segmentation result of the proposed KBA with intensity inhomogeneity.

Table 1: Comparison table of the Our Method, LK Method and LBF Method with the number of iterations and CPU time in seconds.

Image Size	Our Method		LK Method		LBF Method	
	Itr	CPU	Itr	CPU	Itr	CPU
110 × 110	6	0.830	10	0.402	100	6.017395
250 × 250	6	1.418	10	0.342	100	4.434779
350 × 350	6	1.986	10	0.376	100	5.099626
650 × 650	6	6.064	10	0.601	600	26.048569
800 × 800	6	8.199	10	0.750	850	25.987099

The EST J_{σ}^E for a gray image $u_0(\mathbf{x})$ can be defined as follows:

$$J_{\sigma} = K_{\sigma * (\nu \nu^T)} = \begin{pmatrix} K_{\sigma} * u_{0x}^2 & K_{\sigma} * u_{0x}u_{0y} & K_{\sigma} * u_{0x}u_0 \\ K_{\sigma} * u_{0x}u_{0y} & K_{\sigma} * u_{0y}^2 & K_{\sigma} * u_{0y}u_0 \\ K_{\sigma} * u_{0x}u_0 & K_{\sigma} * u_{0y}u_0 & K_{\sigma} * u_0^2 \end{pmatrix}. \quad (3.27)$$

where

$$\nu = [u_{0x} u_{0y} u_0] \quad (3.28)$$

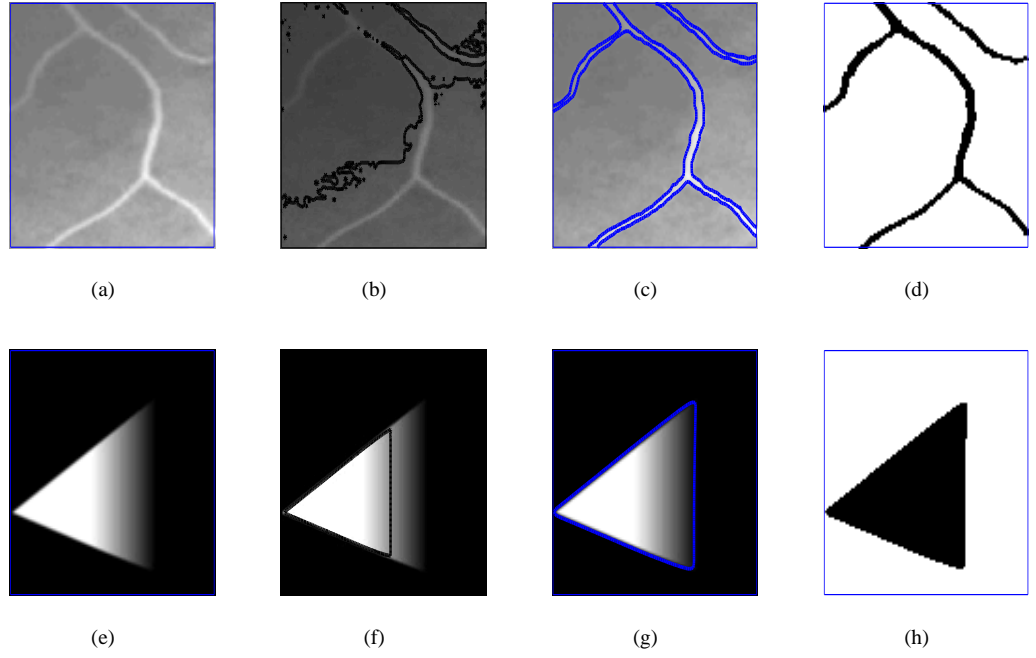


Figure 17: Given figure demonstrates the result of WH and proposed model on two different images suffered from intensity inhomogeneity. First, second and third columns represent the given image, result of WH model and KBA model, respectively. While the forth column shows the segmented result of KBA model.

Following expression for vector-valued images.

$$J_{\sigma}^E = K_{\sigma} * \left(\sum_{i=1}^N \nu_i \nu_i^T, \right) \quad (3.29)$$

where

$$\nu_i = [u_{0i,x} u_{0i,y} u_{0i}]^T.$$

We will first use L_0 smoothing on a given image to remove noisy features and enhance meaningful edges. Next we will apply EST to smooth the textural features for image segmentation.

3.1. **Convexity.** Let us consider the energy functional in Eq.(1.6)

$$F(\phi, c_1, c_2) = \lambda \int_{\Omega} \frac{(C_k \frac{u_0}{u_S} - c_1)^2}{c_1^2} (\phi + 1)^2 \mathbf{d}\mathbf{x},$$

$$+ \int_{\Omega} \frac{(C_k \frac{u_0}{u_S} - c_2)^2}{c_2^2} (\phi - 1)^2 \mathbf{d}\mathbf{x}, \quad (3.30)$$

$$f(z) = \lambda f_A(z) + f_B(z). \quad (3.31)$$

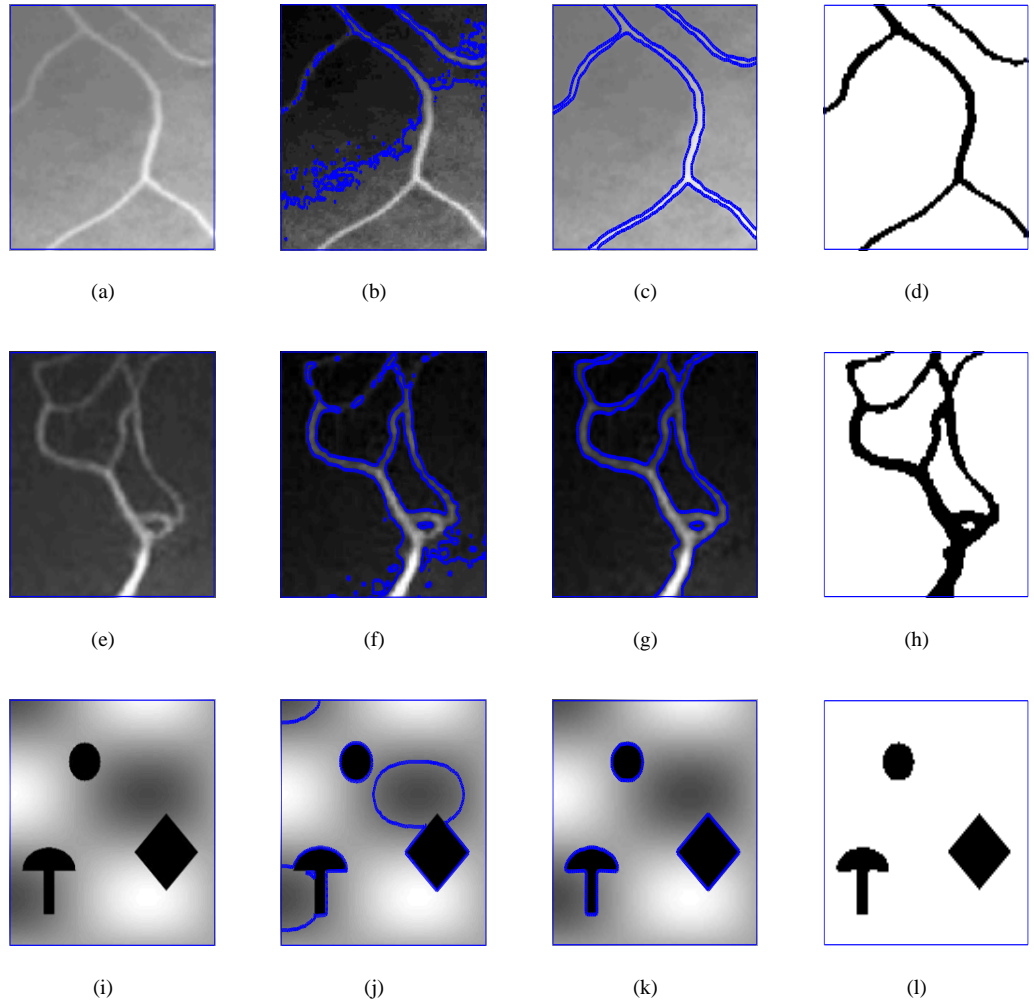


Figure 18: Given figure demonstrates the result of Li-Kim and proposed model on three different images suffered from intensity inhomogeneity. First, second and third columns represent the given image, result of Li-Kim model and KBA model, respectively. While the forth column shows the segmented result of KBA model.

where

$$f_A(z) = \int_{\Omega} \left(\left(C_k \frac{u_0}{u_S} \right) - c_1 \right)^2 \phi H_c(1 + \phi) dz \quad (3.32)$$

And

$$f_B(z) = \int_{\Omega} \left(\left(C_k \frac{u_0}{u_S} \right) - c_2 \right)^2 \phi H_c(1 - \phi) dz \quad (3.33)$$

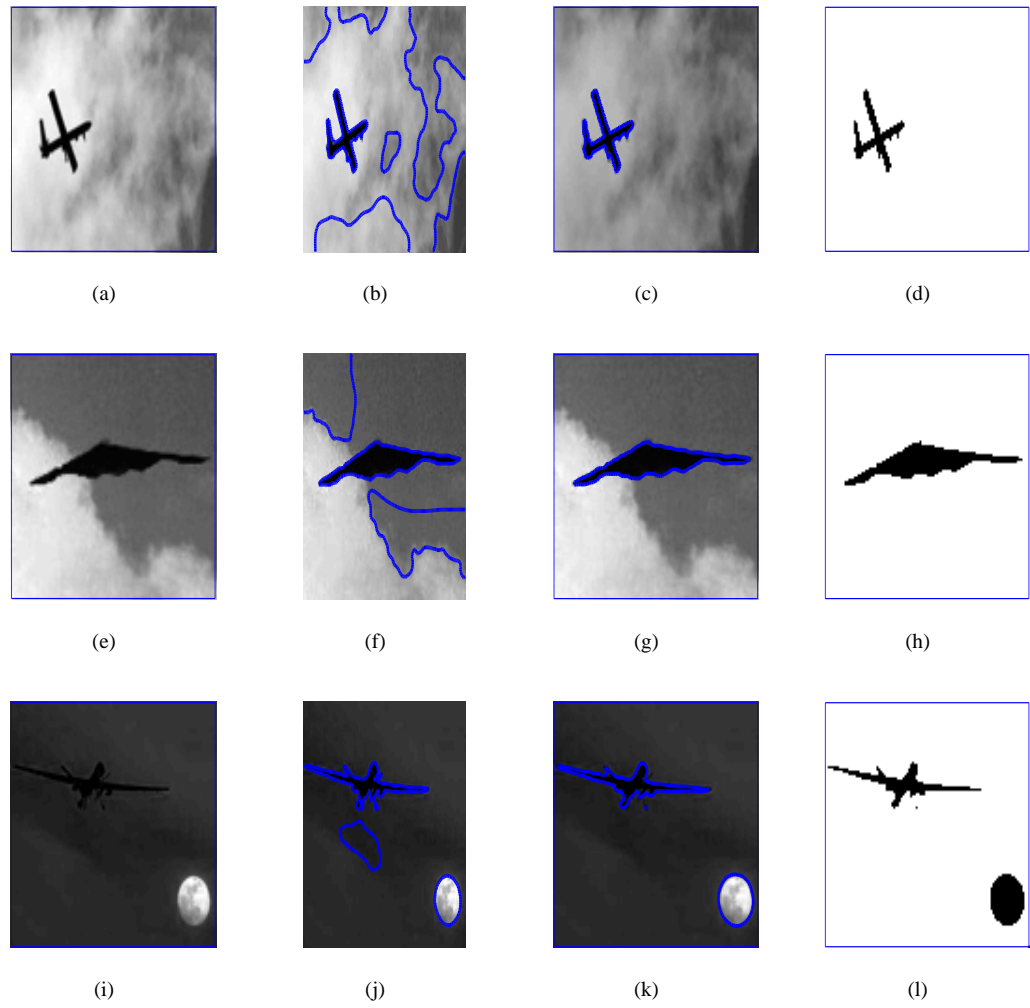


Figure 19: Given figure demonstrates the result of LBF and proposed model on three different images suffered from intensity inhomogeneity. First, second and third columns represent the given image, result of LBF model and KBA model, respectively. While the forth column shows the segmented result of KBA model.

Then $f(z)$ is convex.

Proof:

The functional $f(z)$ is convex for reference see [22] .

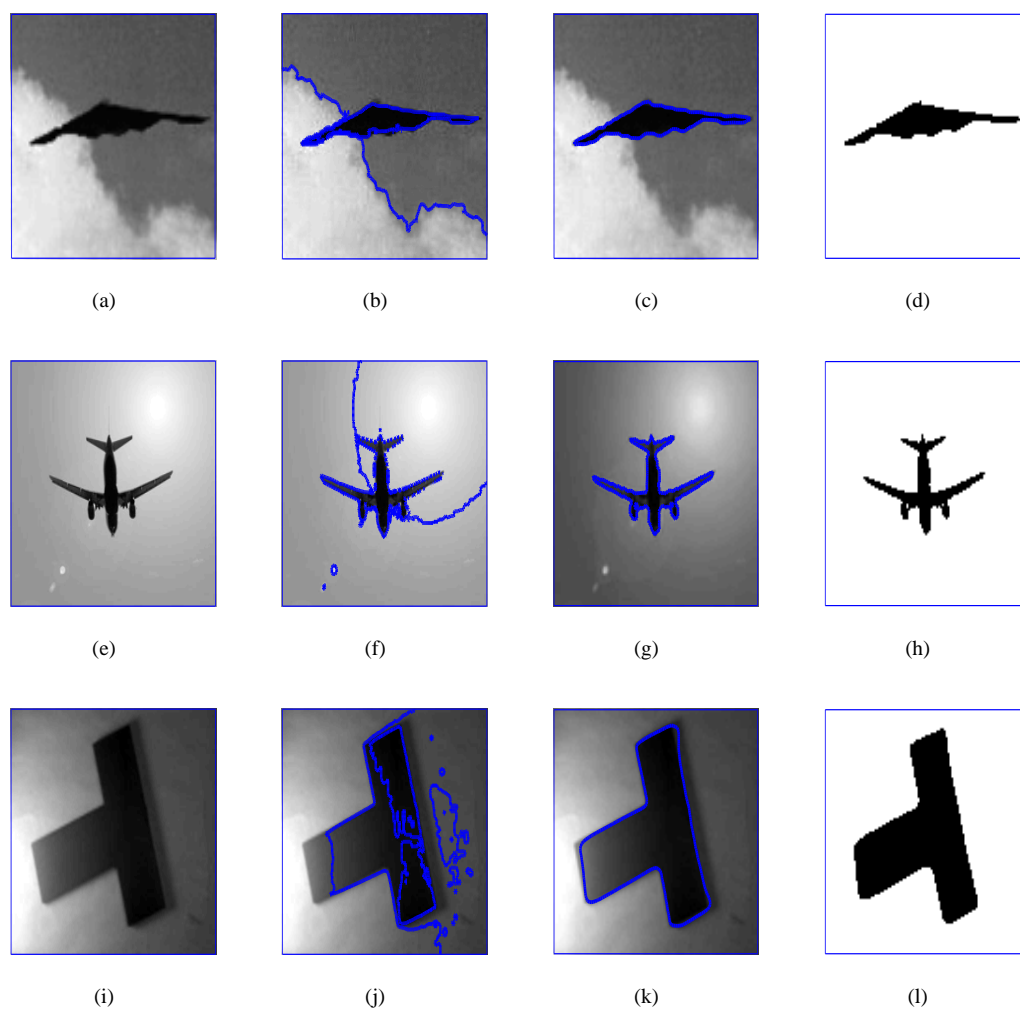


Figure 20: Given figure demonstrates the result of Li-Kim and proposed model on three different images suffered from intensity inhomogeneity. First, second and third columns represent the given image, result of Li-Kim model and KBA model, respectively. While the forth column shows the segmented result of KBA model.

4. EXPERIMENTAL RESULTS

In this section, we present experiments to analyze the performance of our model. We first illustrate the accuracy of the segmentation of the proposed model through different synthetic images. We shows the comparative results of the proposed KBA model with state-of-the-art models, such as LK, WH, LBF and HS models, and shows an over-performance

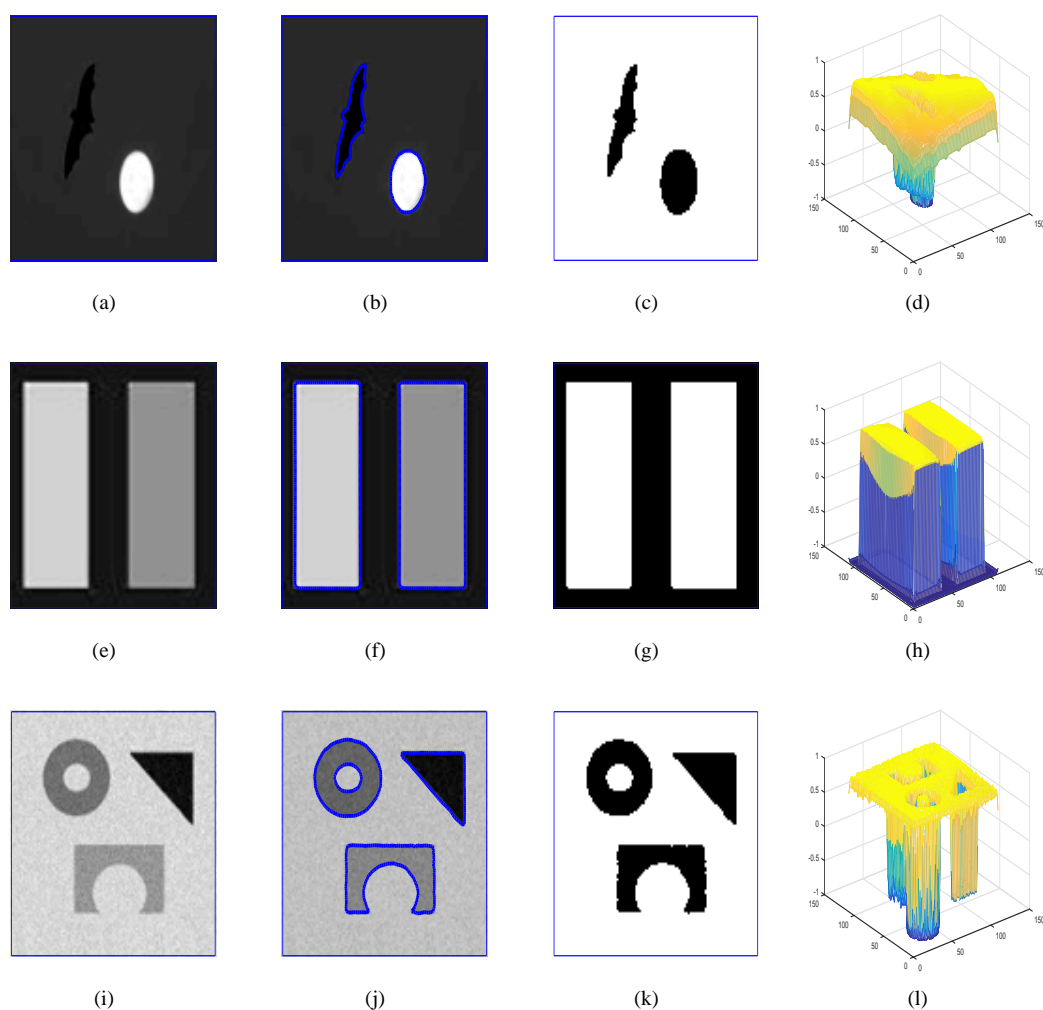


Figure 21: Segmentation result of proposed KBA model on multi-object images .

of the proposed model for real-world images that show complexity due to inhomogeneity, Clutter Background and background brightness. Via experiments, we demonstrate that the proposed method is comparatively faster and much more effective in the segmentation of images with inhomogeneity. Furthermore, the efficiency of the proposed model is also checked in real-world color and texture images.

Test set 1: Correct Segmentation of the Proposed Model.

As shown in Fig.16, segmentation result of our proposed model on a brain medical image with intensity inhomogeneity and also multi-object image with varying intensity levels.

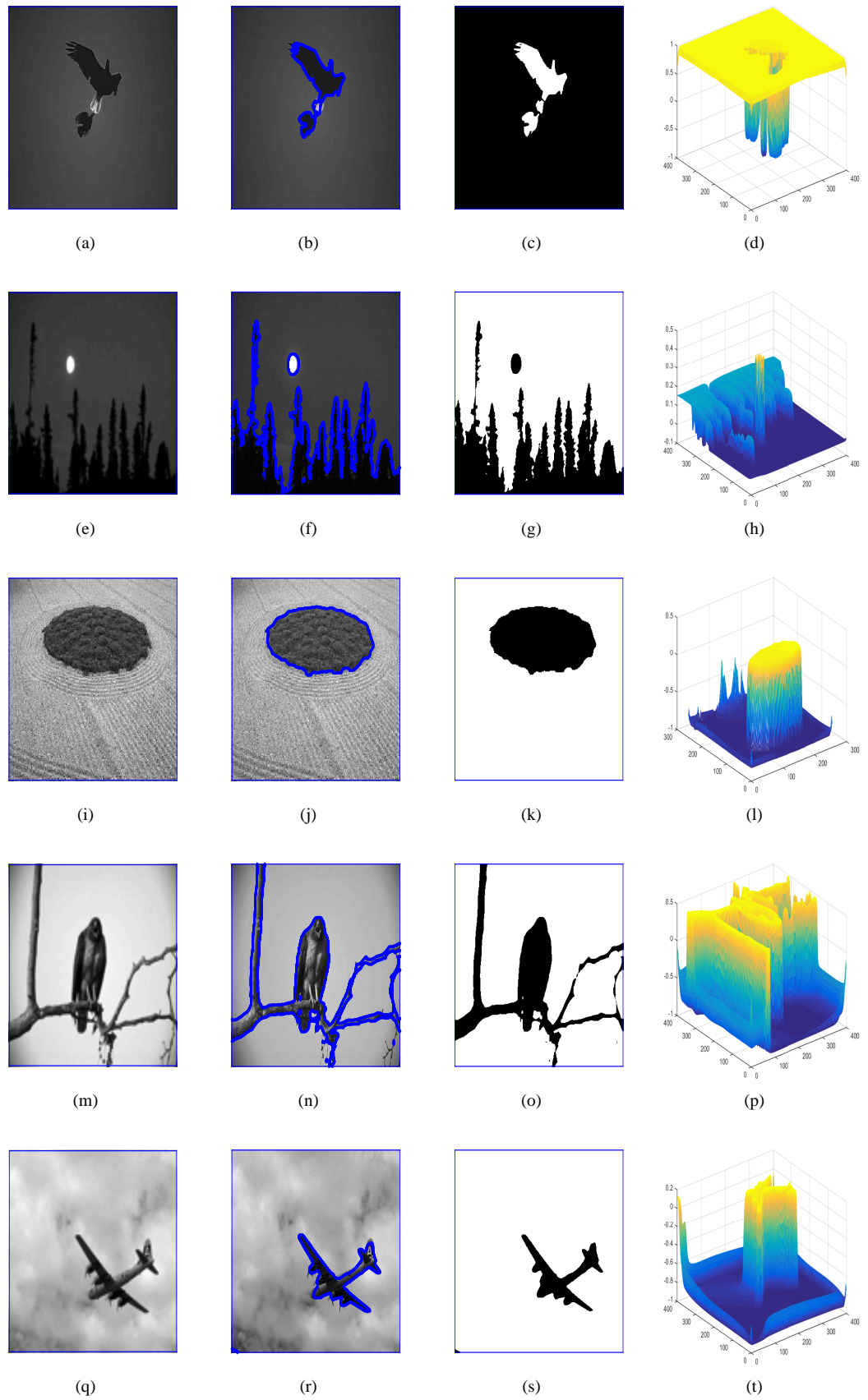


Figure 22: Segmentation result of the proposed KBA model on Berkeley Segmentation Dataset .

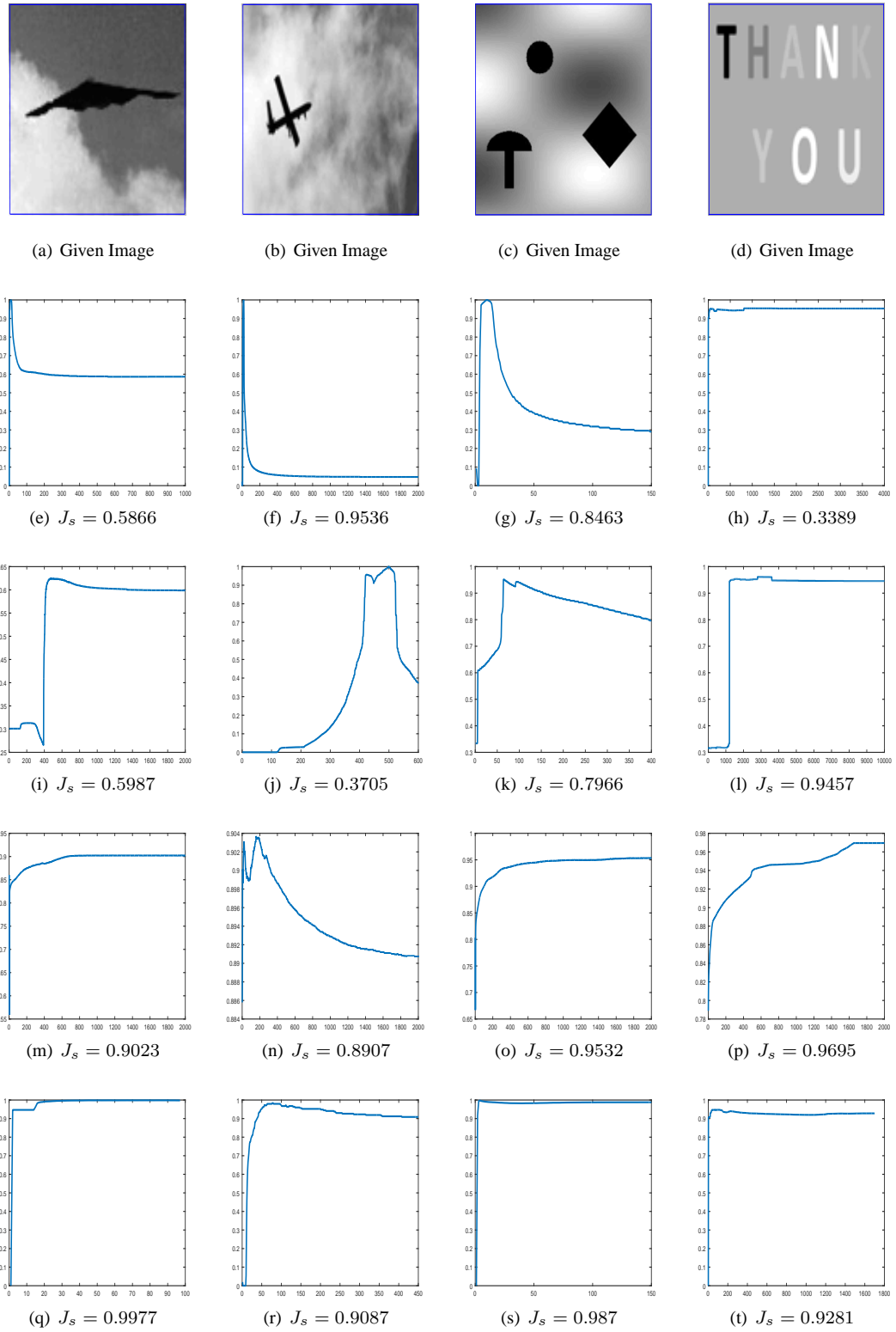


Figure 23: Comparison of four method using Jaccard Similarity. $\{(a,b,c,d)\}$ Original image of size 110×110 ; $\{(e,f,g,h)\}$ results of LK method $J_s = 0.5866, J_s = 0.9536, J_s = 0.8463, J_s = 0.3389$; $\{(i,j,k,l)\}$ result of WH method $J_s = 0.5987, J_s = 0.3705, J_s = 0.7966, J_s = 0.9457$; $\{(m,n,o,p)\}$ result of LBF method $J_s = 0.9023, J_s = 0.8907, J_s = 0.9532, J_s = 0.9695$; $\{(q,r,s,t)\}$ result of KBA method $J_s = 0.9977, J_s = 0.9087, J_s = 0.987, J_s = 0.9281$

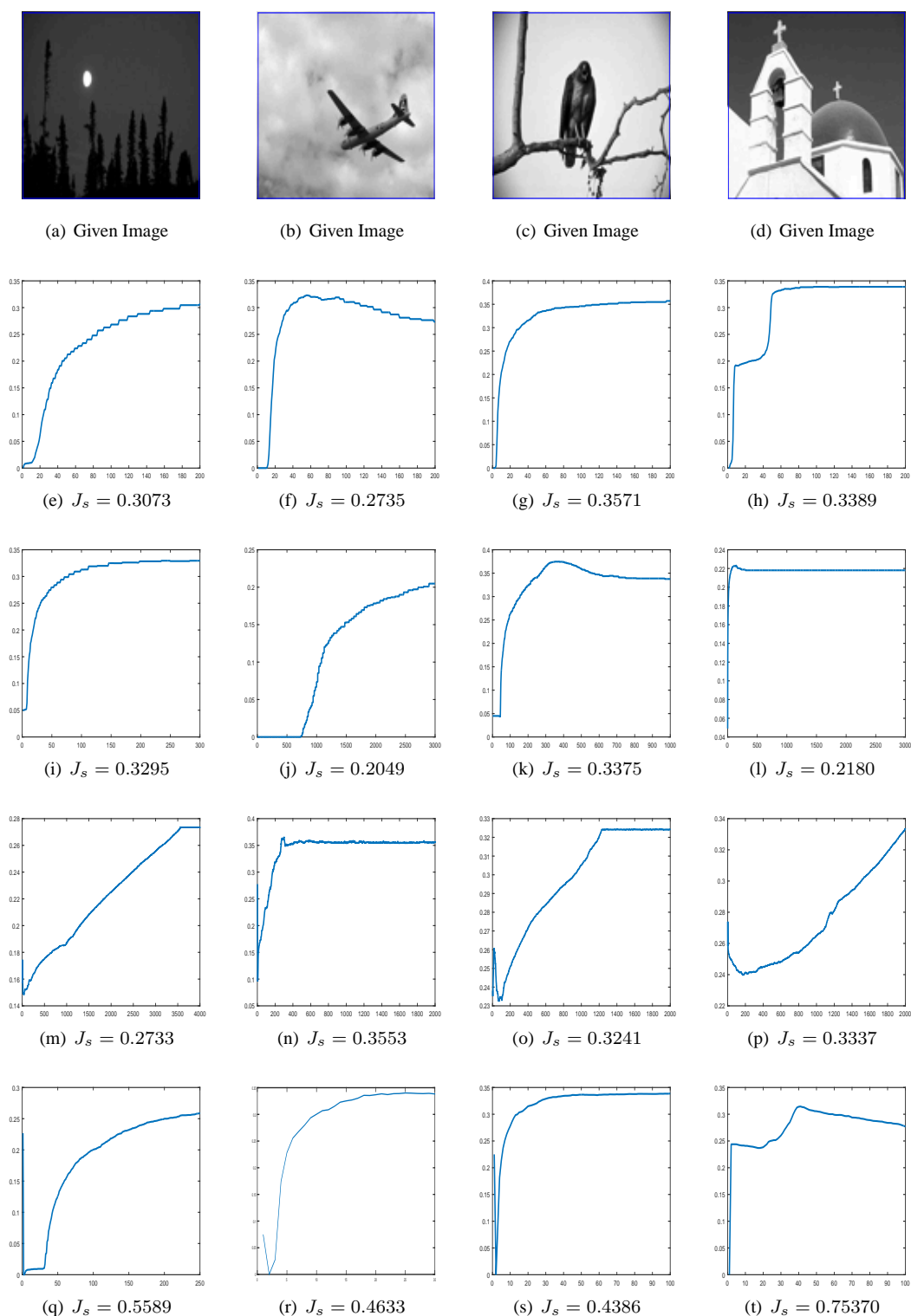


Figure 24: Comparison of four method using Jaccard Similarity. $\{(a,b,c,d)$ Original image of size 110×110 , $\};\{(e,f,g,h)$ results of LK method $(J_s = 0.3073), (J_s = 0.2735), (J_s = 0.3571), (J_s = 0.3389)\};\{(i,j,k,l)$ result of WH method $J_s = 0.3295, J_s = 0.2049, J_s = 0.3375, J_s = 0.2180\};\{(m,n,o,p)$ result of LBF method $J_s = 0.2733, J_s = 0.3553, J_s = 0.3241, J_s = 0.3337\};\{(q,r,s,t)$ result of KBA method $J_s = 0.5589, J_s = 0.4633, J_s = 0.4386, J_s = 0.75370\}$

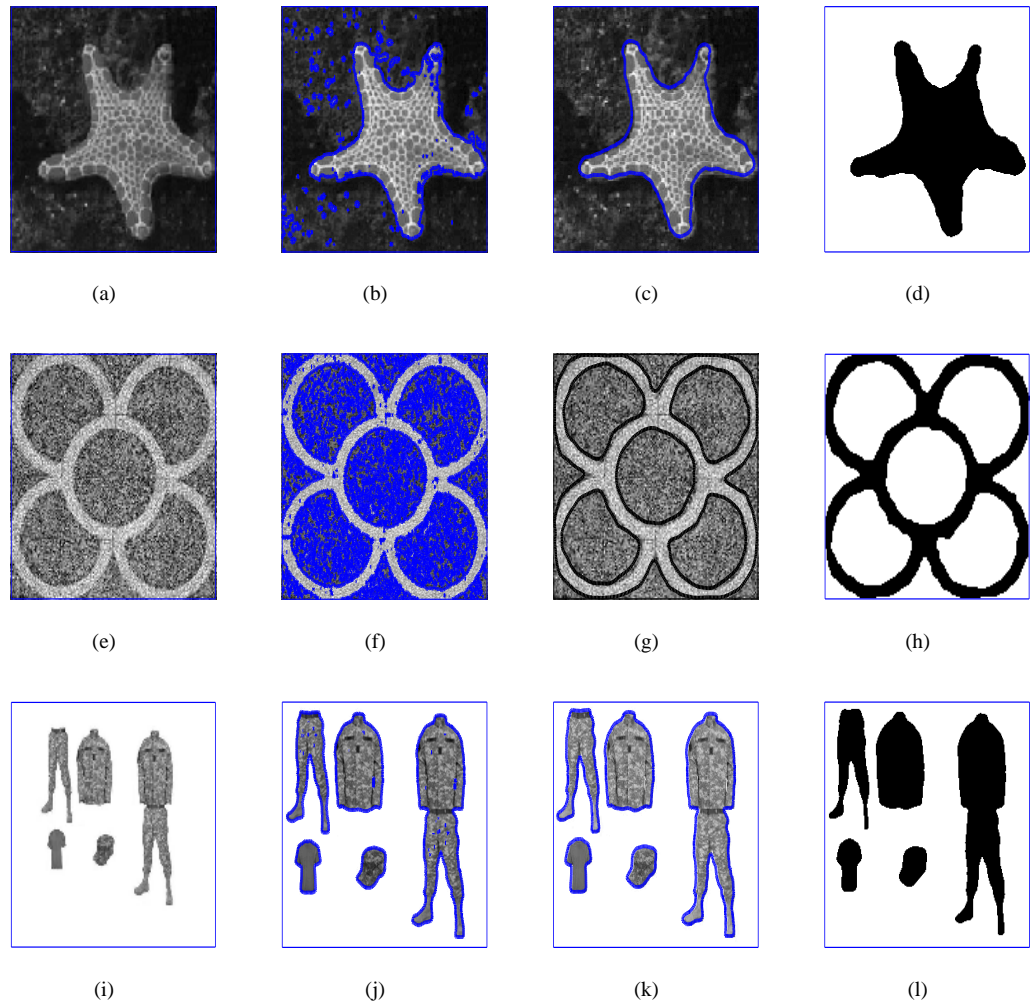


Figure 25: Given figure demonstrates the result of Li-Kim and proposed model on three different images suffered from intensity inhomogeneity. First, second and third columns represent the given image, result of Li-Kim model and KBA model, respectively. While the fourth column shows the segmented result of KBA model.

Test set 2: Comparison of the Proposed Model for Images Suffer from Intensity Inhomogeneity and Images having Clutter Background.

It can be very certainly witnessed that suggested model accurately identified the edges. In Fig. 17 we give test results on an image with intensity inhomogeneity of the proposed KBA and WH models. It can be very easily witnessed that the KBA performs far better than the

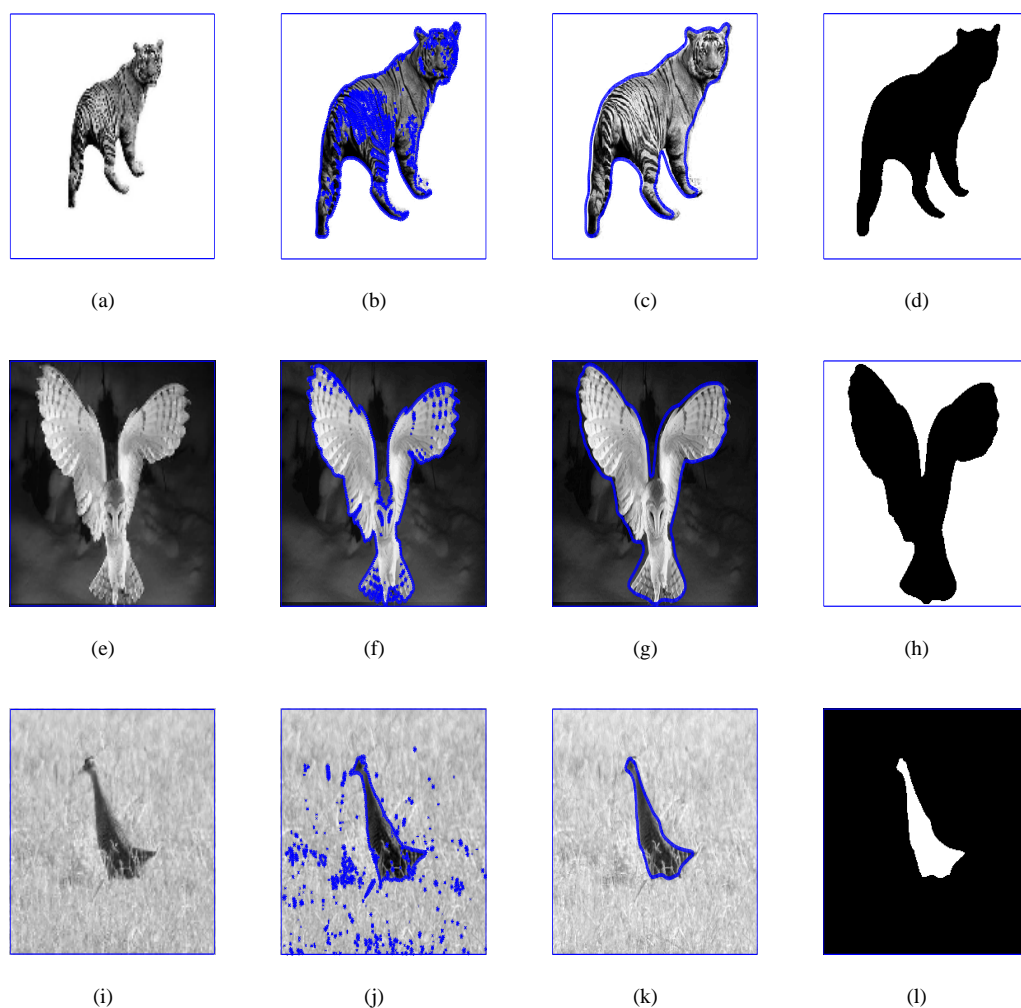


Figure 26: Given figure demonstrates the result of Li-Kim and proposed model on three different images suffered from intensity inhomogeneity. First, second and third columns represent the given image, result of Li-Kim model and KBA model, respectively. While the forth column shows the segmented result of KBA model.

WH model. Next, we evaluate the performance of KBA and LK model in Fig. 18 on image with severe intensity inhomogeneity. It can be observed that the proposed KBA is efficient in accurate segmentation. Next, in Fig. 19 segmentation enactment of our proposed KBA and LBF models on clutter background images are given. From Fig. 19(b), 19(f) and 19(j) we can observe that LBF model segments the objects, However, it also captures some

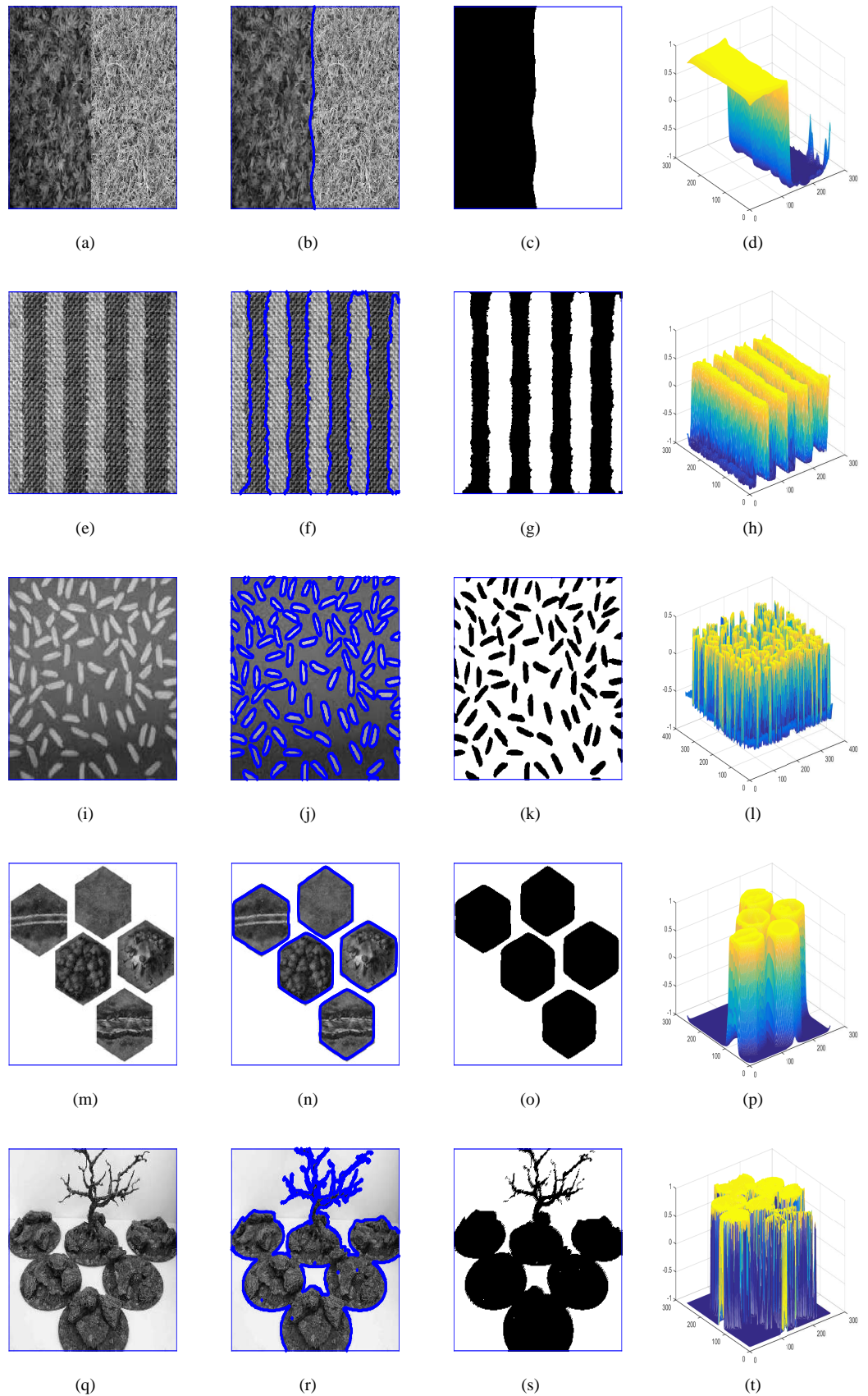


Figure 27: Given figure demonstrates the result of our proposed KBA model on Texture images.

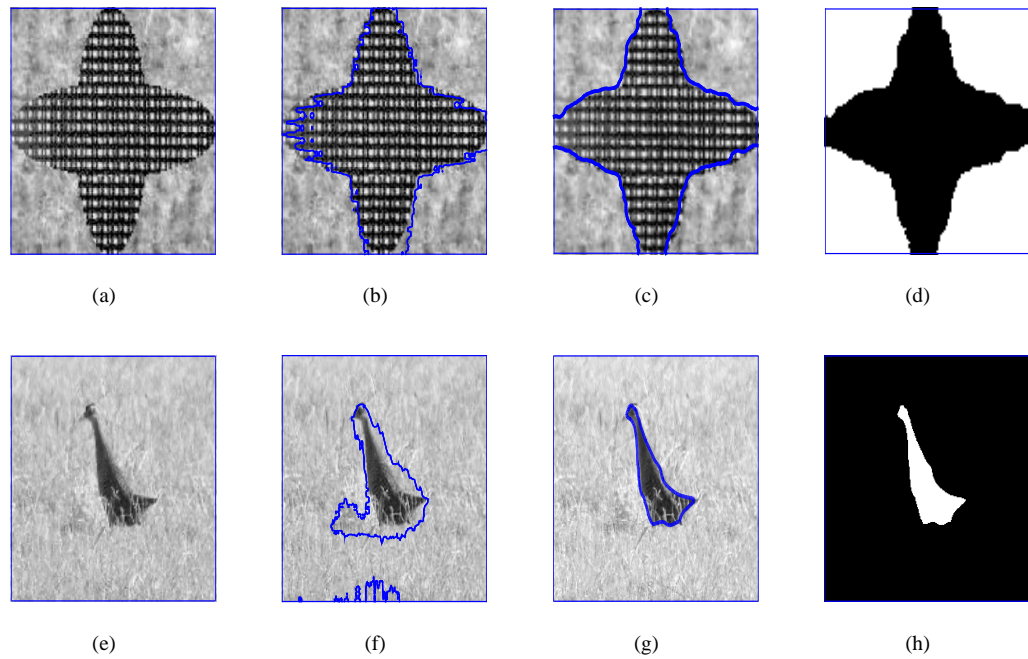


Figure 28: Given figure demonstrates the result of Hassan Shah(HS).[6] and proposed model on two different images suffered from intensity inhomogeneity. First and second columns represent the given image, result of HS model and KBA model, respectively. While the forth column shows the segmented result of KBA model.

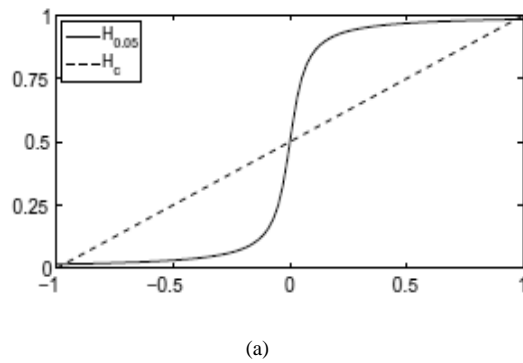


Figure 29: The Heaviside function $H_{0.05}$ and H_c .

parts of the background that show that the LBF model's performance is not satisfactory, while on the other hand, in Fig. 19(c), 19(g) and 19(k) we can see the strong enactment of the KBA model which extract our desire objects. Finally in Fig. 21 we tests our proposed KBA model on multi-objects images. Efficient performance can be very easily observed from the same figure.

Test set 3: Robust performance of the proposed model compare with a Standard Model in Vector-Valued Images having Multi-Region.

To check the efficiency of the proposed algorithm on vector valued images, we compete the proposed VVKBA model and VVCV model on multi-region vector-valued images. In Fig. 15(b), 15(e), 15(h), 15(k), It can very easily observed that result of VVCV model are not satisfactory, on the other hand, Fig. 15(e), 15(f), 15(i), 15(l), show robust enactment of the proposed VVKBA model.

Test set 4: Robust performance of the proposed model compare with a Standard Models in Texture Images.

Furthermore the enactment of our proposed model as to compare to Li-Kim model and Hassan Shah model on texture images can be shown in Fig. 25(c), 25(g), 25(k), and in Fig. 26(c), 26(g), 26(k), and in Fig. 28(c), 28(g).

In Fig. 25 and in Fig. 26 first, second and third columns represent the given image, result of Li-Kim model and KBA model, respectively. While the forth column shows the segmented result of KBA model. Similarly in Fig. 28 first, second and third columns represent the given image, result of Hassan Shah model and KBA model, respectively. While the forth column shows the segmented result of KBA model.

Test set 5: Correct Segmentation of the Proposed Model on Berkeley Dataset and Texture Images.

Robust and accurate segmentation of the proposed model on berkeley data set and texture images can be shown In Fig. 22 and in Fig. 27. In Fig. 22 first, second and third columns represent the given image, result of KBA model and segmented result of KBA model respectively. While the forth column shows the mesh plot of KBA model respectively. Similarly in Fig. 27. first, second and third columns represent the given image, result of KBA model and segmented result of KBA model respectively. While the forth column shows the mesh plot of KBA model respectively.

Test set 6: Jacard Similarity of the Proposed and Rest of the Models.

The enactment of the proposed model on synthetic images and Berkeley Dataset images as compare to the Li-Kim, Wu-He, LBF as shown in Fig. 23(q), 23(r), 23(s), 23(t) and 24(q), 24(r), 24(s), 24(t).

At Fig. 23 jacard similarity value of Li-Kim, Wu-He, LBF and our proposed KBA are $J_s = 0.5866, J_s = 0.9536, J_s = 0.8463, J_s = 0.3389$; $J_s = 0.5987, J_s = 0.3705, J_s = 0.7966, J_s = 0.9457$; $J_s = 0.9023, J_s = 0.8907, J_s = 0.9532, J_s = 0.9695$; and $J_s = 0.9977, J_s = 0.9087, J_s = 0.987, J_s = 0.9281$ respectively. Likewise at Fig 24 jacard similarity value of Li-Kim, Wu-He, LBF and our proposed KBA are $(J_s = 0.3073), (J_s = 0.2735), (J_s = 0.3571), (J_s = 0.3389)$; $J_s = 0.3295, J_s = 0.2049, J_s = 0.3375, J_s = 0.2180$; $J_s = 0.2733, J_s = 0.3553, J_s = 0.3241, J_s = 0.3337$; and $J_s = 0.5589, J_s = 0.4633, J_s = 0.4386, J_s = 0.75370$ respectively.

Images Comparison table of the Our Method, LK Method and LBF Method with the number of iterations and CPU time in seconds 1

5. CONCLUSION

In this paper we proposed a novel segmentation model for multi-region image segmentation with intensity inhomogeneity. Based on dual filter formulation and efficient level set technique, the proposed model has shown better results on hard images. The experiments on some synthetic and real images have shown that our proposed method of segmenting images with multi-regions and intensity inhomogeneity is effective and robust. The contrasts with the model LBF, the model Li-Kim and the model Wu-He also demonstrate the superiority of the proposed method over traditional methods based on the local region. In addition, the proposed algorithm retains the accuracy on texture and vector-valued images.

6. ACKNOWLEDGMENTS

First of all I am grateful to almighty Allah who helped me to carry out this research work. I am heartily thankful to my supervisor Dr. Noor Badshah, who guided me in every step of my research work. His kind supervision helped and motivated me all the time. I can not forget Dr. Haider Ali, who also helped me where I needed him. Finally, my thanks go to all the people who have supported me to complete this research work directly or indirectly.

REFERENCES

- [1] H. Ali, N. Badshah, K. Chen, G.A. Khan and Z. Nosheen, *Multiphase segmentation based on new signed pressure force functions and one level set function*, Turkish Journal of Electrical Engineering and Computer Sciences. DOI: 10.3906/elk-1606-260, 2016.
- [2] H. Ali, N. Badshah, K. Chen, G.A. Khan, *A variational model with hybrid images data fitting energies for segmentation of images with intensity inhomogeneity*, Pattern Recognition, **51** (2016)27-42.
- [3] N. Badshah, K. Chen, H. Ali, G. Murtaza, *A coefficient of variation based image selective segmentation model using active contours*, East Asian J. Appl. Math. **2**, (2012) 150-169.
- [4] . Badshah and K. chen, *Multigrid method for the chan-vese model in variational segmentation*, Comm. Comput. Phys. **4**,No.2(2008):294-316
- [5] N. Badshah and K. Chen, *Image selective segmentation under geometrical constraints using an active contour approach*, Commun. Comput. Phys. **7**,No.4 (2009) 759-778.
- [6] N. Badshah and H. Shah, *Model for smoothing and segmentation of texture images using L_0 norm* IET Image Processing . (2017).
- [7] X. Bresson, S. Esedoglu, P. Vandergheynst, J-P. Thiran and S. Osher, *Fast global minimization of the active contour/snake model*, J. Math. Imag. Vis., **28**, No.2 (2007) 151-167.
- [8] T. F. Chan and L. A. Vese, *Active contours without edges*, *IEEE Transactions on Image Processing*, **10**, No.2 (2001) 266-277.
- [9] Xiao-Feng Wang,Hai Min, Yi-Gang Zhang, *Multi-scale local region based level set method for image segmentation in the presence of intensity inhoogeneity*, Neurocomputing, **151** (2015) 1086-1098.
- [10] Li C, Huang R, Ding Z, et al., *A level set method for image segmentation in the presence of intensity inhomogeneities with application to MRI*, *IEEE Transactions on Image Processing*, **20**,No.7 (2011) 2007-2016.
- [11] C. Li, C. Xu, C. Gu, M.D. Fox, *Level set evolution without re-initialization a new variational formulation*, *IEEE Conf. Computer Vision and Pattern Recognition*,**1** (2005) 430-436.
- [12] C. M. Li, C.Y. Kao, j. C. Gore, Z.H. Ding, *Implicit active contours driven by local binary fitting energy*, *Proceeding of CVPR*, **07** (2007)1-7.
- [13] Y. Li, J. Kim, *An unconditionally stable numerical method for bimodal image segmentation*, *Apple. Math. Comput.* **2**,No.19(2012) 3083-3090.

- [14] L. Mabood, H. Ali, N. Badshah, Ke Chen, G. Ali Khan, *Active contours textural and inhomogeneous Object extraction*, Pattern Recognition, **55** (2016) 87-99.
- [15] D. Mumford and J. Shah, *Optimal approximation by piecewise smooth functions and associated variational problems*, Communications on Pure Applied Mathematics, **42**(1989)577-685.
- [16] J. A. Sethian, *Level set methods and fast marching methods*, Evolving interfaces in Computational Geometry, Fluid Mechanics, Computer Vision and Material Science, Cambridge University Press, Londres. 1999.
- [17] L. Vese, T. Chan, *A multiphase level set framework for image segmentation using the Mumford and Shah model*, Int. j. Comp. Vis. **50**, No3 (2002):271-293.
- [18]
- [19] L. A. Vese and T. F. Chan, *A multiphase level set framework for image segmentation using the Mumford and Shah model*, Int. J. Computer Vision, **50**,No.3 (2002) 271-293.
- [20] U. Vovk, F. Pernus, B. Likar, *A review of methods for correction of intensity inhomogeneity in MRI*. IEEE Trans. Med. Imaging, **26**, No.3 (2007) 405-421.
- [21] X.-F. Wange, D.-S.Huange, H. Xua, *An efficient local chan-veese model for image segmentation*, Pattern Recognition, **43**, No.3 (200) 603-618.
- [22] Y. Wu,C. He, *A convex variational level set model for image segmentation*. Singal processing, **106**(2015) 123-133.